Title

Recent advances in integrated solid-state nanopore sensors.

Journal

Lab on a Chip, 21(16)

Authors

Rahman, Mahmudur
Sampad, Mohammad
Hawkins, Aaron
et al.

Publication Date

2021-08-21

DOI

10.1039/d1lc00294e

Peer reviewed

HHS Public Access

Author manuscript

Lab Chip. Author manuscript; available in PMC 2022 August 21.

Published in final edited form as:

Lab Chip. 2021 August 21; 21(16): 3030–3052. doi:10.1039/d1lc00294e.

Recent advances in integrated solid-state nanopore sensors

Mahmudur Rahman[a,b], **Mohammad Julker Neyen Sampad**[a], **Aaron Hawkins**[c], **Holger Schmidt**[a]

[a]University of California, Santa Cruz, Santa Cruz CA, 95064 USA.

[b]Dhaka University of Engineering & Technology, Gazipur, Bangladesh.

[c]Brigham Young University, Provo UT, 84602 USA.

Abstract

The advent of single-molecule probing techniques has revolutionized the biomedical and life science fields and has spurred the development of a new class of labs-on-chip based on powerful biosensors. Nanopores represent one of the most recent and most promising single molecule sensing paradigms that is seeing increased chip-scale integration for improved convenience and performance. Due to their physical structure, nanopores are highly sensitive, require low sample volume, and offer label-free, amplification-free, high-throughput real-time detection and identification of biomolecules. Over the last 25 years, nanopores have been extensively employed to detect a variety of biomolecules with a growing range of applicatons ranging from nucleic acid sequencing to ultrasensitive diagnostics to single-molecule biophysics. Nanopores, in particular those in solid-state membranes, also have the potential for integration with other technologies such as optics, plasmonics, microfluidics, and optofluidics to perform more complex tasks for an ever-expanding demand. A number of breakthrough results using integrated nanopore platforms have already been reported, and more can be expected as nanopores remain the focus of innovative research and are finding their way into commercial instruments. This review provides an overview of different aspects and challenges of nanopore technology with a focus on chip-scale integration of solid-state nanopores for biosensing and bioanalytical applications.

Graphical Abstract

Conflicts of interest

H.S. and A.R.H. have financial interest in Fluxus Inc. which commercializes optofluidic technology. The remaining authors declare no competing interests.

†Footnotes relating to the title and/or authors should appear here.

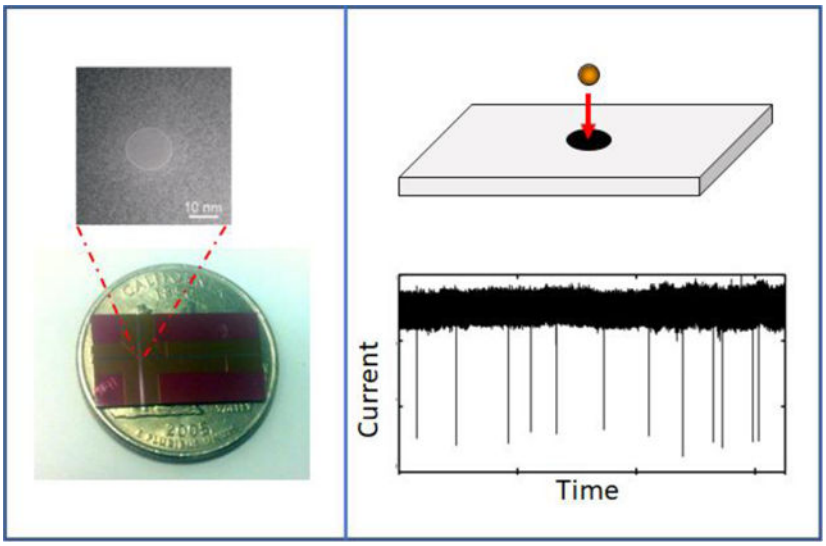

Nanopores are powerful single molecule sensors that have a wide range of applications from single molecule biophysics to medical diagnostics. This review covers all aspects of nanopore sensor integration into increasingly complex lab-on-chip systems.

1 Introduction

Detection and analysis of single molecules has become a key tool for improving our understanding of biological and biochemical processes at the molecular level. Moreover, this ultimate level of sensitivity is increasingly being used as the basis of next generation instruments for disease diagnostics, precision medicine, and improved healthcare[1–8]. Nanopore research has seen an explosive growth in this context due to their potential use as target agnostic, label-free molecular detectors and their function as selective elements for other types of sensors[9–17]. A nanopore is a nanometer-scale hole formed by a natural protein or artificially defined in a thin membrane[18–22]. Conceptually, it is, therefore, the molecular-scale version of the Coulter counter developed by Wallace Coulter during the 1940s[23]. Coulter counters are used to count microscopic objects such as red blood cells by passing them through a hole of comparable size one by one. The Coulter counter has two compartments filled with ionic solution that are separated by a membrane which contains a microscopic hole (~10μm). The application of a bias voltage establishes an ionic current and whenever a red blood cell passes through the hole, it partially blocks the hole. This blockade manifests as a reduction of the ionic current that heralds the passage of the cell through the pore. Nanopores can be visualized as a Coulter counter with nanoscale dimensions and a nanosize pore instead of the microscale aperture and more precise current measurement tools[9,24].

The nanopore concept was first introduced by D. Deamer in 1989[25] and experimentally demonstrated in 1996[18]. Initially, nanopore research was focused virtually exclusively on nucleic acid sequencing based on the idea that different nucleotide bases would generate different blockade signals[21,26,27]. Over time and partially driven by the development of advanced nanofabrication methods, nanopores have been increasingly employed to

probe a variety of biomolecules such as single-stranded (ss) DNA[28–34], double-stranded (ds) DNA[28,35–40], RNA[41–44], proteins[45–49], ribosomes[45,50,51], viruses[52,53], peptides[54–56], enzymes[57–59], biomolecular complexes[60–63], and a vast pool of nanoparticles[64–68]. Furthermore, nanopore technology has evolved towards more general molecular analysis platforms, including smart gate molecular delivery tools[45,69–75], mass spectrometers[76–78], for energy harvesting[79–81], thermoscopy[82], etc.[24]. Over the past three decades, nanopores have been rigorously and actively studied around the world among a diverse group of disciplines including but not limited to electrical, computer, biomedical, and mechanical engineering, biology, material science, physics, chemistry, medicine, proteomics, and genomics, thereby making it a highly interdisciplinary field[14,24,83].

A variety of single-molecule probing techniques, diagnostics, and clinical methodologies have already been developed based on optical, electronic, microfluidic, and optofluidic techniques[84–89]. The marriage between nanopore technology and the other existing methodologies is paving the way for low-cost, complete, chip-scale, portable single-molecule probing, and diagnostic tools. The integration of microfluidic labs-on-chip with nanopore technology is fusing two very powerful techniques in a single platform. Leveraging advantages from either approach has already delivered a number of exciting results[90–94]. Microfluidic systems can offer contamination-free on-chip low volume sample preparation and purification steps prior to delivering target molecules to the nanopore for a thorough analysis. Low sample loss, hermetic sealing of the system, temporal and spatial control of the target molecules inside the chip can increase the nanopore detection efficiency and specificity[91,92,95]. Moreover, the incorporation of powerful electronic automation[96] and multichannel microfluidic chip design[97] enable parallel and multiplexed detection in nanopore arrays. Furthermore, nanopores are suitable for integration with electronic and CMOS technology, thereby showing potential towards commercial mass production of compact, personalized, point of care diagnostic tools[98–100]. Probably, the most powerful and advanced type of nanopore integration is with optical techniques. Optical methods have recently seen increased levels of integration as optofluidics has popularized the combination of microfluidics and integrated photonics in a single chip-scale system and is finding applications in numerous fields including life science, biosensing, and diagnostics [101–105]. Therefore, the integration of nanopores with optical methods is timely and a natural next step. Numerous breakthroughs and interesting results have already been reported such as multimodal (simultaneous electrical and optical detection) detection[52,106–112], nanopore capture rate enhancement[45,69], cell transfection[113,114], force measurements on DNAs[74,115–117], and plasmonic nanopores that greatly enhance the nanopore sensitivity[75,111,118]. This review aims to provide an overview of the current status of nanopore sensor integration as powerful labs-on-chip. It is organized as follows. First, we give an overview of the fundamentals of the nanopore sensing concept and nanopore fabrication methods. Next, different examples of integrated nanopore devices, with a special focus on chip-scale integration and separated by topical area, are discussed. The review concludes with a look at the current state of the art, challenges, and future prospects for integrated nanopore platforms.

2.1 Nanopore working principle

Fig. 1 (a) illustrates the working principle of a nanopore sensor. The nanopore connects the “cis” and “trans” sides of a thin, non-permeable, electrically insulating membrane. Both sides of the membrane are filled with an ionic solution (KCl, NaCl, etc.). An electrical bias voltage with proper polarity is applied across the pore using a pair of electrodes (typically Ag/AgCl) as shown in Fig. 1 (a), resulting in a constant baseline ionic current flow through the pore. Biomolecules on the cis side that are contained within a capture radius of typically a few microns around the pore experience large electric fields and are pulled to the trans side of the pore. This disruption produces a transient spike in the ionic current, which is generally considered as the confirmation of molecular translocation[19,21,26]. The transient current modulation may result in a decrease or increase in the ionic current depending on the salt concentration and chemical environment[40,119,120]. We will refer to these electric signatures as blockades, regardless of the sign of the current change. The physical properties (e.g. size, shape, charge) of a biomolecule are encoded within the translocation signal, which can be further analyzed and digitally processed to distinguish among different biomolecules within a mixture[45,52,121,122]. The signal can also be analyzed to resolve notable natural and artificial features within a biomolecule such as DNA knots[35,36], molecules bound with DNAs[60,62], drug delivery[41], digital encoding[63], etc. If the current blockades from individual DNA bases can be distinguished, it is possible to read the DNA sequence as it passes through the pore in a linear fashion. This forms the basis of nanopore DNA sequencing [26,121,123,124] and most of the early work in the field focused on next-generation sequencing applications. This vast area is outside the scope of this review, but the reader is referred to several independent reviews on nucleic acid sequencing that can be found elsewhere[125–129].

2.2 Nanopore categories

In general, nanopores can be classified into three broad categories-biological, solid-state, and hybrid nanopores. Biological nanopores are highly ordered macromolecular biostructures that are found in nature. Most of the biological nanopores are either protein channels such as α-hemolysin[130], MspA[131], aerolysin[132], ClyA[133], FluA[134], Omp F/G[135,136], and CsgG[137], or viral connectors such as phi29[138], SPP1[139], T3[139], and T4[139]. Fig. 1 (b) shows the cross-sectional view of the α-hemolysin pore that was used in the original proof of the nanopore sensing concept in 1996[18]. Due to the high precision in size and shape, biocompatibility, and low inherent noise, biological nanopores are widely used for probing DNA, RNA, polymers, polypeptides, etc.[26,140–142]. Additionally, Oxford Nanopore Technologies has already commercialized the first DNA sequencing prototype based on a mutant CsgG pore and some other companies are on their way to developing nanopore-based sequencers[143,144]. Despite numerous advantages, biological nanopores have some crucial drawbacks such as fixed pore size, poor mechanical stability, limited lifetime, and non-reusability which in turn limits the integration of biological nanopores as an LoC component[19,83,145].

To mitigate these issues, for the last two decades, researchers have focused their expertise on exploiting micro and nanofabrication techniques for fabricating artificial nanopores. Recent advancements in nanotechnology have made it possible to develop artificial nanopores on thin solid-state membranes.

The first of these synthetic or solid-state nanopores (ssNPs) was reported in 2001 by Li et al. [146]. These nanopores are durable and robust, allow tunable pore size, have better mechanical stability, have better compatibility with the experimental environment, are mass-producible, and can be parallelized in nanopore arrays, making them an attractive candidate for versatile and commercial applications[14,145,147]. Most importantly, ssNPs can be integrated with other technologies to take advantage of a complete chip-scale device[45,52,148]. Fig. 1 (c) shows a typical SEM image of a ssNP. As a suitable alternative to their biological counterpart, solid-state nanopores are widely and actively employed for nucleic acid sequencing, detecting proteins, monitoring protein interaction, drug delivery, probing a pool of nanoparticles, smart gating and controlled molecular delivery[14,45,149–151].

As biological and solid-state nanopores have their own pros and cons, researchers have come up with some elegant ideas to insert biological nanopores into ssNPs to form hybrid nanopores. The mechanically stable ssNP supports the fragile biological nanopore, which has precise size and shape to probe biological particles with inherently low noise, thus combining the advantages from both structures. In 2010, Hall et al. reported the formation of a hybrid nanopore by directly inserting an α-hemolysin pore into an ssNP as shown in Fig. 1 (d)[152]. They functionalized the α-hemolysin nanopore with a 3kbp dsDNA via a 12nt long oligomer and then electrophoretically drove it to a ~3nm ssNP so only the stem of the α-hemolysin pore fit in the nanopore, with the ds-DNA passed through the pore. To verify the functionality of the hybrid pore, ss-DNA was introduced and successfully detected using the hybrid pore. Cressiot et al. also reported a similar approach to form a hybrid nanopore by combining a natural DNA pore from a thermostable virus into a solid-state SiN nanopore[153]. In 2012, an alternative way of forming a hybrid nanopore was reported by combining DNA origami with ssNPs[154]. DNA origami enables 3D shaped nanostructures with high precision nanopore geometry[155]. Since solid-state nanopores are much more compatible with device integration in a lab-on-chip format, we will focus on this type of implementation in the remainder of this review.

3 solid-state nanopore fabrication

Solid-state nanopore device fabrication comprises several steps such as preparing a thin solid-state membrane, perforating that membrane to create a nanoscale opening (nanopore), and addition of easily accessible fluidic cells and metallic electrodes for introducing analyte solution to both sides of the pore and driving those target particles through the pore, respectively. Moreover, integrating a nanopore platform in a lab-on-chip format includes additional steps such as definition of fluidic channels, optical waveguides, embedded electrical circuits etc. However, in this section we will focus on different techniques for the core step of opening a nanoscopic aperture in a thin membrane. The sensitivity and quality of the nanopore detection signal fundamentally depend on the physical structure of the nanopore. Therefore, nanopore fabrication and the overall pore geometry play a crucial role in nanopore functioning, detection limit, and sensitivity. Also, the combined choice of the membrane, material, and fabrication technique offer researchers different ranges of size, shape, and surface properties of the nanopore. Depending on the application, different materials have been tested as nanopore membrane, including SiN, SiO_2, TiO_2, Al_2O_3, ZnO, HfO_2, BN, MoS_2, and graphene[149,156,157]. As a special note regarding probably the

most commonly used membrane material, SiN, or silicon nitride, this material is typically produced by chemical vapor deposition and may come in the stoichiometric form of S_3iN_4 or in a form that may include excess hydrogen, typically designated as SiN_xH_y. In this review paper, whenever we refer to silicon nitride, we will use the generic abbreviation SiN, which may or may not refer specifically to Si_3N_4. For nanopore fabrication, there is a pool of choices available, including ion beam or electron beam milling, chemical etching, dielectric breakdown, nanopipette by pulling glasses, nanoimprinting, and thermal annealing.

3.1 Ion beam and electron beam milling and sculpting

This method is probably the most popular and conceptually straightforward way of fabricating solid-state nanopores. A focused beam of ions/electrons with high energy (in the range of thousands of electron-volts) strikes the thin membrane into which the nanopore is to be milled. As the ions/electrons carry a massive amount of energy they start eroding the thin membrane by removing the surface atoms, a process called milling. As the process continues, eventually the focused ion beam (FIB)/ focused electron beam (FEB) pierces through the membrane creating a hole in the membrane. A variety of ion beams have been used for this purpose, including He^+, Ga^+, Ne^+, Ar^+, Kr^+, and Xe^+[157]. One may not end up with the expected nanopore size in the first step due to the intrinsic limitation of ion beam size[146,158,159]. Therefore, in a subsequent step, the nanopore diameter can be fine-tuned using a process called nanopore shrinking which is essentially slow deposition of materials to shrink the pore to the expected size[146,160].

The incorporation of the ion beam sculping technique for solid-state nanopore fabrication was pioneered by Li et al. in 2001[146]. Fig. 2 (a) depicts a schematic representation of this methodology. The nanopore was milled on a free-standing SiN membrane with a bowl-shaped cavity in the substrate below it as shown in Fig. 2 (a). A high energy Ar^+ beam was irradiated on the flat side (opposite side of the cavity) of the membrane to create a molecular size pore. An ion counter was set under the membrane with a feedback control system to stop the sculpting process at the appropriate moment. The nanopore diameter is further reduced from ~60nm to ~1.8nm by ion beam assisted material deposition. Since this demonstration, focused ion beams have been extensively used in nanopore fabrication[161]. In FIB milling, nanopore precision significantly depends on the ion beam diameter, shape, redeposition, and without shrinking, usually yields a nanopore diameter of more than 10 nm[160,161]. However, the use of a helium ion microscope (HIM) has proved to be a useful tool as it has a higher resolution compared to the Ga^+ ion beam and nanopores in the range of 4 nm have been fabricated using HIM[162,163]. Apart from the FIB, the focused electron beam of a transmission electron microscope (TEM) has also been explored for milling sub 10nm pores. Due to the beam size, FEB yields better precision and facilitates the fabrication of smaller nanopores compared to the FIB milling process[164–168]. Storm et al. reported the fabrication of sub 10 nm pores using the FEB milling method in 2003[169]. Using scanning TEM, ultrasmall subnanometer pores (~0.3nm) have been fabricated as reported by Kennedy et al.[170,171]. Although it requires expensive tools and trained personnel, the FIB/FEB milling method remains the most popular method of choice due to its precision, reproducibility, high resolution, and ease of patterning, [145,149,157,161].

3.2 Dielectric breakdown

In simple terms, dielectric breakdown usually means the failure of an insulating/dielectric material to withstand an applied electrical field. When a voltage comparable to the dielectric strength of a thin membrane is applied across it, the localized carriers form a tunneling current through the membrane. As a result, the membrane starts to get physically damaged and eventually a small aperture opens and a nanopore is formed. Kwok et al. pioneered the development of nanopore fabrication following the controlled dielectric breakdown (CDB) technique[172]. The schematic representation of their nanopore fabrication process using CDB method is depicted in Fig. 2 (b). In their study, a thin SiN membrane was immersed in an aqueous solution (1M KCl) and mounted in a liquid cell forming two separate chambers. A custom built feedback amplifier was used to apply the breakdown voltage across the SiN membrane via Ag/AgCl electrodes following a standard technique. Nanopores as small as 2nm were fabricated using this method and can be enlarged upon application of further voltage. To test the fabricated nanopore functionality, ds DNAs with different lengths were detected using these nanopores. In a separate study, Waugh et al. reported a protocol to fabricate nanopores following CDB in an automated fashion[173]. A modified method of CDB to fabricate nanopore was proposed by Yanagi et al. who used a pulse train of different levels to form the nanopore[174]. Using this method, nanopores with 1–2 nm diameter were fabricated which can be widened with subnanometer precision. The CDB technique has also been used for nanopore fabrication in different studies[175–180]. One significant advantage of this method is the simplicity and inexpensive setup. Additionally, this method enables in-situ fabrication of nanopores which avoids random contamination. In contrast, CDB is not a suitable technique for nanopore fabrication on membranes thicker than ~30 nm and devices with special structures such as optofluidic devices[14]. Also, precise positioning of nanopore location is difficult and the exact shape of a fabricated nanopore may not be guaranteed which in turn affects the reproducibility[14,172].

3.3 Nanopipettes

The nanopipette concept originated from the micropipettes used in cell cytology[156]. A nanopipette is essentially a glass capillary with a nanoscale hole at the tip which looks similar to a usual pipette tip, however, at a quite smaller scale. Fig. 2 (c) shows an SEM image of a nanopipette fabricated by Karhanek et al.[181]. The process starts with a thin-walled quartz capillary with an inner diameter of 700μm and an outer diameter of 1mm. A programmable laser-based pipette puller (P-2000) was used which essentially melts the capillary using the laser beam and then pulls the capillary from two ends to form the nanopipette. This produced nanopipettes with a diameter ranging from 37 nm to 82 nm, but other groups reported smaller diameter nanopipettes[156,182,183]. Although this is the most common method for fabricating nanopipettes, other methods are also reported such as two-step glass pulling[184], or carbon nanotube tipped pipettes[185]. However, it is hard to achieve sub 10 nm diameter openings in a nanopipette[149]. For typical nanopore experiments, the nanopipettes are filled with suitable buffer solutions and an electrode is inserted into the stem of the nanopipette. The nanopipette itself also emerges into the bulk electrolyte solution where the second electrode is placed for applying the bias voltage across the pipette opening. Over the past two decades, nanopipettes have become an important tool for sensing and analysis of biomolecules.

3.4 Chemical etching method

Chemical etching is a widely used process in standard silicon fabrication[186]. Researchers have taken advantage of this readily available technology to fabricate nanopores. As illustrated in Fig. 2(d), Park et al. defined an inverted pyramid (using a sharp tip) on one side of a silicon wafer whereas the other side was chemically etched (KOH) to form a truncated pyramid [187]. As shown in Fig. 2 (d), the chip was mounted in an electrochemical setup that separates a KCl solution chamber and KOH solution chamber while the sharp inverted pyramid is kept in KCl solution. Using two Pt electrodes, the current through the two solution chambers was monitored with an application of bias voltage (~800 mV). A sharp increase in the current was considered as the indication for successful pore formation. The slow KOH etch rate (~18 nm/ min) enabled manual stopping of the etch process once a pore was formed. After some post chemical treatment, bi-pores of 10 nm and 28 nm diameters, respectively, were formed (Fig. 2 (d) inset). Other studies have reported a nanopore fabrication process utilizing a similar chemical etching method[188,189]. A variation of this approach is the two-step track etching method, where in a first step, high-energy metal ions are bombarded on the membrane to create the tracks. In the following step, the membrane is chemically etched which removes the damaged tracks faster compared to the intact parts and eventually creating nanopores[31,190–193]. Chemical etching facilitates parallel nanopore fabrication which is attractive for mass production. However, improving the resolution remains a challenge[161].

4 Integrated nanopore devices

Integrated technology allows for creating miniature devices that fuse different, powerful capabilities in a single, chip-scale platform. Lab-on-chip devices have embraced the wafer-scale integration paradigm first developed in the electronics industry[194–196]. Recently, nanopores are also being integrated with such LoC devices, which makes nanopore-based sensing more practical, adds capabilities which are not present in bulk experiments, and improves the performance of capabilities already implemented in bulk. An overview of the state of art and recent advances in integrated nanopore devices is given in the following sections.

4.1 Microfluidic integration with nanopores

Microfluidic devices are one of the common platforms for bioanalysis as it is imperative to ensure a fluidic environment for biomolecules for their proper functioning. Furthermore, in most of the cases, biomolecular analysis requires pre-processing of samples, guided flow etc. which can be achieved using a microfluidic platform[197–199]. Due to the advancement of microfabrication, microfluidic devices are utilized for chemical and biological analysis of analytes at a very small scale and volume[200,201]. Also, the addition of actuation in the microfluidic systems using mechanical valves and electrokinetic forces enables on-demand particle flow and mixing in a sealed environment[202–204]. Furthermore, microfluidics and optics can also be fused together to facilitate both fluidic and optical manipulation in a single “optofluidic” platform[102–105]. Up to now, several studies on microfluidic and optofluidic integration with nanopores have been reported with an increasing range of research and applications[52,94,205,206].

4.1.1 Electrical sensing—The most natural use of nanopores in a lab-on-chip format is as an integrated version of their original vision as electrical particle sensors. Usually, microfluidic devices are designed based on soft lithography techniques applied to materials such as Polydimethylsiloxane (PDMS). This technique enables rapid device prototyping that is affordable, offers easy multilayer stackings, embedded electrodes and better controllability of particle flow inside the fluidic channels[207–209]. Several groups have reported nanopore integration with a hybrid structure that mainly consists of a PDMS device whereas the nanopore is incorporated on a Si based thin membrane at the heart of the device[94]. This hybrid integration was pioneered by Kuo et al. who developed a filtering and particle delivery platform depending on the particle size[210]. In their study, a nanopore array was formed following the track etched method that was used for transferring particles in a three-dimensional fluidic network. Contemporary studies have been performed in similar 3D fluidic networks with integrated nanopore to observe the effect of electro-osmotic and electrophoretic forces induced by a nanopore[211]. Using a simple modular process based on transfer printing, Jain et al. introduced an integrated nanopore microfluidic platform to detect single DNA molecules[212]. This remarkably improved the nanopore signal to noise ratio as the inherent nanopore noise was reduced by minimizing the fluidic contact area of the Si membrane and, thus, the membrane capacitance. Gradually, with improved techniques, different application-oriented designs of integrated nanopore microfluidic platforms have been developed. Fig. 3 (a) shows a schematic representation of an integrated nanopore microfluidic platform designed and developed by Roman et al.[93]. In their study, an intelligent way to bond Si based nanopore membrane with a PDMS microfluidic platform was devised that can be reused with bond reversal to overcome the limitation of sealing the nanopore membrane permanently and irreversibly onto the PDMS device. Moreover, the fluidic channels were formed using a low-cost 3D printed mold on a PDMS film followed by a 3D graphics mold design. For nanopore integration, a 20 nm thick SiN membrane with a 200 μm thick Si substrate was used. On the SiN membrane, a ~30 nm nanopore was milled using a TEM which resulted in pore diameters between 3 – 200 nm. Their PDMS subunits were partially bonded using two stage plasma bonding and the nanopore membrane was inserted into the top PDMS layer through an aperture formed by a biopsy puncher. A special form of PDMS was cast to ensure proper sealing, which can withstand a pressure of 2 bar without leaking. The top and side view of the whole device are depicted in Fig. 3a (i) and a picture of a fabricated device is shown in Fig. 3a (ii). The remarkable feature of this scheme is that the nanopore membrane is not permanently bonded but hermetically sealed with the PDMS film, so it is possible to reuse the membrane in different PDMS devices or alter the membrane with a different nanopore in the same PDMS device. This platform was utilized to understand the polymer-based model of protein-urea interactions on the nanometric scale and the results were in agreement with previous demonstrations[93].

Apart from nanopore integration with PDMS based microfluidic devices, nanopores can also be integrated with Si based microfluidic and optofluidic devices. In 2010, Holmes et al. reported a novel approach to incorporate nanopores seamlessly with microscale fluidic channels[213]. The device contains a “Z” shaped liquid-core (LC) channel with interconnected solid-core (SC) optical waveguides as depicted in Fig. 3 (b). In this study, they developed

a two-step nanopore fabrication process. In the first step, the thick top oxide layer on the LC channel was etched using reactive ion etching (RIE) down to a 200nm thick chrome etch stop layer, forming a ~4μm hole and leaving a thin SiN membrane suitable for milling the nanopore. In the next step, the nanopore was defined using the FIB milling method and the nanopore diameter was fine-tuned depending upon the target size. Subsequently, an alternative approach to mill the nanopore using the dual beam scanning electron microscope (SEM) alone was developed[160]. Here, to remove the top oxide layer and forming the thin membrane, FIB sculpting instead of RIE etching was used[160]. Different nanopore fabrication and sculpting methods for this type of device were compared in a rigorous study [160]. For biosensing applications, the presence of the microfluidic channel allows for the introduction of sample solution via the reservoirs attached to the two ends of the channel. Additionally, samples can be electrophoretically driven to the LC channel through the nanopore using a third reservoir glued on top of the nanopore. In a separate study, the nanopore functionality was validated by detecting 50S ribosomal subunits moving through a 45 nm pore which was the first demonstration of ribosome detection using a nanopores[50]. Moreover, Parks et al. introduced the concept of hybrid microfluidic integration with an optofluidic device[214,215] which may be integrated with nanopores to facilitate further microfluidic manipulation like on-chip automated sample preparation, labeling, and delivery towards a complete and portable lab-on-chip application[215–217].

In addition to microfluidic integration with nanopores, electronic integration and control methodologies have recently become popular among nanopore researchers. Electronic integration, especially CMOS integration with nanopore sensing has the potential to take advantage of the well-developed electronics economy of scales in the electronic industry and may culminate in chip-scale applications. [98,218]. Recently, companies such as Oxford Nanopore Technology, Roche etc. are developing nanopore sequencing devices combining powerful electronics for fast DNA/RNA sequencing[144,145,219].

4.1.2 Multichannel architecture and parallel detection—As microfluidic devices can route multiple channels in a controllable fashion, it is also possible to integrate multichannel devices with nanopores. The prospect of multichannel devices is one of the key drivers for incorporating nanopores on a lab-on-chip device as this can facilitate parallel operation, faster processing and potential multiplexed detection in rapid succession[94,220,221]. Tahvildari et al. reported the integration of nanopore arrays with a multichannel microfluidic device[97] by processing a commercial Si chip to prepare a 20 nm thick SiN membrane. The membrane was then mounted within a PDMS microfluidic device having five independent fluidic channels on the top layer and a common microfluidic channel at the bottom as shown in Fig. 4 (a). For fluidic and electrical access, holes were punched at the top and bottom microfluidic channels. To fabricate individual nanopores on the five fluidic channels, they precisely localized the electric potential within a single microchannel and fabricated single nanopores using the controlled dielectric breakdown method. The leakage current through the SiN membrane was continuously monitored during the process. The opening of the pore was heralded by a sudden abrupt increase in the current and the applied voltage was then cut off within 0.1 s. To validate the functionality of this 5 × 1 nanopore array, they detected ds-DNA and human α-thrombin protein through the nanopores. One

potential application of such a multi-pore, multichannel scheme is to deliver targets into a specific microchannel on an on-demand basis. As additional examples of parallel detection, Bell et al. demonstrated simultaneous detection of ds-DNAs in 12 individual nanopipette channels which can potentially be boosted up to 16 channels[222]. Yanagi et al. also reported a similar multichannel approach for simultaneous detection of analytes[90]. Recently, Zeng et al. designed a microfluidic platform with an array of nanopores that provides multiplexing functionality in which each nanopore can be addressed individually[223].

4.1.3 Electrokinetic fluidic control—Microfluidic devices can be designed to leverage electrokinetic fluid manipulation to preconcentrate target particles close to the nanopore capture volume (target capture region of a nanopore). This preconcentration increases the nanopore translocation frequency and improves the limit of detection for sensing target particles at ultralow concentrations[210]. Recently, Spitzberg et al. demonstrated an integrated nanopore microfluidic platform that can increase the event frequency based on an electrokinetic fluid manipulation method referred to as isotachophoresis (ITP)[92]. ITP is a method of selectively focusing and separating ionic analytes using two different buffer solutions having different mobilities. For lab-on-chip implementation, they designed a custom built PDMS chip that had a long microfluidic channel (~20mm) with a free-standing SiN membrane. Fig. 4b (i) depicts a schematic view of the device with different layers and assembly details. Using a micropositioner, the PDMS microchannel was aligned with the SiN membrane and clamped together using a magnet. Fig. 4b (ii) shows the top view of an assembled device with fluidic and electrode access. After assembling the device, a sub 10 nm pore was fabricated on the SiN membrane using the CDB method which facilitates in-situ nanopore fabrication. For ITP focusing, they used terminating and leading electrolyte buffers and applied a bias voltage of 100 V. Fig. 4b (iii) shows a top view of the ITP channel, and Fig. 4b (iv) illustrates the cross-section of the PDMS channel with an integrated nanopore. As the device was made of transparent PDMS and a glass slide, it was possible to visualize and estimate the sample focusing factor in real time by observing the fluorescence produced by optically tagged target molecules. Once the ITP reached the nanopore zone, the ITP bias was manually turned off and the nanopore measurements were activated using a separate electrical setup. Using this method, the authors were able to achieve a ~337-fold increase in event rate compared to the nanopore only case. Apart from the ITP based fluid flow manipulation, researchers studied the effect of fluid flow on nanopore translocation process that provides important insight about the particle capture process at different flow conditions[224].

4.1.4 On-chip sample preparation and detection—One notable feature of microfluidics is the complete on-chip, automated sample preparation for solid phase nucleic acid or protein extraction from biological fluids[225–228]. Therefore, nanopores can potentially be integrated with sample preparation platforms for a complete on-chip diagnostic tool. Varongchayakul et al. reported an integrated microfluidic platform with nanopores that offers on-chip sample preparation, purification and nanopore measurements in a single platform[91]. Schematics of the structure, chip assembly and a photo of a picture are shown in Fig. 4 (c). The device features a microfluidic sample preparation chamber with heat-resistant Zeonex plastic and a nanopore sensing chip connected with fast-curing PDMS sealant. The

on-chip sample preparation chamber has a multiport liquid handling mechanism connected with programmable syringes, an analyte isolation chamber (50 μl reaction volume) with a magnet assisted analyte separation facility as well as a reaction chamber with PID controlled heating block that can withstand a temperature up to 75°C. After necessary filtration, the platform can deliver specific target particles to the nanopore capture volume without any airborne contamination and evaporative sample loss as these functions take place in a closed system. The minimum sample volume that this system can analyze and manipulate is 10 μl. To validate the device functionality, they demonstrated on-chip 5kbp DNA purification with silica coated magnetic nanoparticles from a crude PCR sample in approximately 15 minutes. The nanopore functionality was verified by detecting 5kbp DNAs and the translocation results were found to be in good agreement with conventional nanopore experiments. The integrated nanopore microfluidic platform with versatile sample processing and detection capability with low volume fluid manipulation can pave the way towards a low limit of detection, on-chip, portable, point of care diagnostic tool.

4.2 Optical integration with nanopores

Optical methods are probably the most versatile and widely used techniques to probe biomolecules, especially at the single molecule level[85,229–231]. They offer non-invasive and contact-free manipulation which are ideal for sensing biomolecules in fluidic media[232–234]. Recent developments in optical techniques such as fluorescence imaging, trapping, or optical tweezing have started a renaissance in probing and manipulating biomolecules. Optical methods also offer additional integration capabilities which is highly desired for boosting nanopore technology. Therefore, integration of nanopore sensing with optical methods very popular when offers a wide range of applications with rapidly growing demand[52,95,149,235].

4.2.1 Translocation control—Slowing down the speed of translocation is of great interest in nanopore studies especially, in nucleic acid sequencing and detecting small analytes[236,237]. Controlling the translocation speed is one of the major challenges in nucleic acid sequencing and several studies have addressed this issue[237–241]. Fiori et al. reported an optical method to slow down the analyte speed based on reversible optoelectronic control of the surface charge of a solid-state nanopore without altering the geometry of the pore or permanently changing the surface characteristics[242]. They milled the nanopore into a SiN membrane and mounted it on a teflon holder forming the cis and trans side of the nanopore. For optical integration, a custom confocal microscopy setup was used to illuminate the nanopore with a 532 nm laser. This modified the nanopore surface charge and, thus, the electroosmotic flow through the pore. Fig. 5 (a) shows a schematic representation of the laser illuminating a nanopore which in this case doubled the ionic current. This dynamic surface control is capable of slowing down the translocation speed and enabling researchers to detect and analyze small but highly charged protein molecules such as ubiquitin. Using this method, the authors were able to slow down the DNA translocation speed by an order of magnitude. Additionally, they reported that illumination of the nanopore can unclog a clogged pore without requiring removal of the chip and subsequent chemical cleaning. As the laser induced heating is insignificant, the authors believe that photoconductivity is responsible for the effects, which they found depends on the e-beam dosage during the

nanopore milling. As this method can slow down the speed of DNA translocation, it may have significant importance in DNA sequencing applications.

4.2.2 On-chip sorting and manipulation of DNA—On-chip sorting and uncoiling of DNAs have many potential applications in bioanalysis including DNA sequencing[243,244]. Zrehen et al. devised an intelligent way to sort and electro-optically detect ultra-long DNAs after uncoiling[245]. Their study was designed on a complex chip structure which has SiN pillar structures followed by a funneled microchannel. The authors use a low temperature anodic bond to bind the SiN membrane with glass. Due to the delicate anodic bonding, it was necessary to use an in-situ nanopore fabrication method. In this case, the authors used a nanopore fabrication method called laser-etching which facilitates diffraction limited control to precisely position and fabricate a nanopore at the center of the microchannel. The authors reported sequence specific optical labelling and on chip sorting and stretching of very long DNA molecules that can offer researchers both synchronous capture and optical imaging of the target DNAs in order to have a better control over translocation behaviour. A schematic representation of their methodology is depicted in Fig. 5 (b). The DNAs were loaded into the device with an application of negative pressure that starts elongating the coiled DNA. Next, the SiN pillars provide an entropic barrier for the ultralong DNA that results in significant elongation of the DNAs before moving to the nanopore entrance. Also, the funnel shape channel right after this pillar structure ensures that the stretched DNA molecules are delivered at the proximity of the pore. Using this method, the authors showed 80% stretching of a 400kbp DNA molecule and more than 3x magnitude of translocation slowdown compared to the nanopore without any nanopillar integration. Moreover, they demonstrated labelling of specific DNA segments by nick translation. Depending on the fluorescence color obtained during the imaging process, one can sort the DNA by altering the vacuum pressure right before these molecules enter the nanopillar structure. The demonstration of stretching very long DNAs with a slowed down translocation speed may create avenues in DNA sequencing as well as sensing applications.

4.2.3 Multi-modal detection—Optical methods can also be directly integrated with nanopores for simultaneous electro-optical detection. Different groups have reported such simultaneous electro-optical detection of tagged particles using different techniques such as top-down microscopy[109], epifluorescence[111], TIRF[246], and planar waveguide-based detection[52,247]. Combined electro-optical detection enables additional analytical modalities for particle detection, increases the confidence of detection, and possibly offers alternative solutions to address challenges in current nucleic acid sequencing[52,109]. In a usual electro-optical detection method, a single analyte is first electrically detected using the nanopore and subsequently detected using an independent optical method. Therefore, one transient signal is obtained from the electrical detection whereas another is generated from the optical fluorescence detection. Assad et al. devised an approach to resolve the temporal and spatial detail of a translocating DNA by analyzing the fluorescence signal originating from single DNA molecules encoded with multiple colors[248]. They milled a 3 nm nanopore on a 15 nm thinned SiN membrane using the TEM milling method. The nanopore chip was mounted on custom CTFE cells with Ecoflex 5 silicone rubber. For optical integration, a custom built confocal microscopy setup with dichroic mirrors was used to separate and

route the excitation and fluorescence signal to corresponding optical paths. For optical tagging, five monocolor custom designed molecular beacons were hybridized to a single DNA. While translocating through the nanopore, the unzipped beacons produced five distinct fluorescence bursts when excited with the optical laser light which is intuitively expected. The optical fluorescence was only found when followed by the electrical detection spikes, confirming that the fluorescence bursts were coming from the barcoded DNAs rather than any spurious events. Next, the DNAs were encoded with two different color tags (red and green in this case; total 5 tags) with a specific color coded sequence. This time, the resulting fluorescence bursts confirm the color coded sequence, thus validating the core concept of dual mode sensing. Fig. 5 (c) depicts a schematic representation of the electro-optical detection methodology with a representative electrical and optical detection signal. To implement this method, the main challenge was to tackle the high photoluminescence background emerging from the SiN membrane that contained the nanopore. The photoluminescence was reduced by exposing the membrane to an electron beam after thinning it using reactive ion etching. This reduction in background optical signal significantly improved the SNR and enabled the authors to resolve the color coded fluorescence signals originating from single DNAs. This electro-optical detection of color-coded single DNAs can potentially provide sufficient spatial resolution to distinguish among different nucleotides, thereby paving the way towards ana electro-optical nucleic acid sequencing platform.

4.2.4 Force spectroscopy—Ashkin's demonstration in 1970 that light can transfer momentum upon collision with small particles shifted the paradigm in bioanalysis[249]. This transfer in momentum exerts a force on the particle, opening the door for non-invasive mechanical particle manipulation. The most common implementation for single bioparticle analysis is a tightly focused laser beam that can trap and levitate small enough particles at the tightest point, often referred as an optical tweezer[250]. In 2006, Keyser et al. reported a study where they incorporated optical tweezers with a nanopore that can measure the electrical force exerted on a single DNA[117]. A custom-built inverted microscope setup was designed for optical integration as depicted in Fig. 6 (a). A diode pumped Nd: YAG laser (1064 nm) was used for optical trapping, and a red diode laser (635 nm) was used to determine the position of the optically trapped particle. The nanopore was milled on a solid-state membrane using a TEM. The nanopore membrane was then mounted on a PDMS-based flow cell as schematically represented in Fig. 6 (a). Target DNAs were attached with ~2 μm functionalized beads using standard procedure. The nanopore was localized by scanning the focused IR laser on the nanopore membrane. When the laser spot coincided with the nanopore location, an increase in ionic current was noticed due to the heat-assisted increase in ionic conductivity. After localizing the nanopore, they trapped a single target carrying bead at the focal spot of the optical tweezer. The trap was calibrated by observing the power spectrum. Upon application of a nanopore bias voltage, they controllably inserted a single DNA into the nanopore. The reflected light from the bead and membrane was used to measure the bead position. As the trap was calibrated and the bead position was identified, they were able to measure the electrical force exerted on the DNA upon an application of voltage. Sischka et al. reported similar studies where they manipulated single λ-DNAs and measured the force exerted on the single DNA[251]. Hout et al. also reported a

similar study where they determined the net force on a single dsRNA molecule[116]. Bell et al. used optical tweezers to analyze the translocation dynamics based on the geometry of nanopore[74].

4.2.5 Cell transfection—Optical tweezers are also employed for cellular analysis using nanopores. Some researchers reported the integration of solid-state nanopores with optical particle manipulation methods that can perform cell transfection via electroporation[113,252]. In simple terms, cell transfection is a process of deliberately inserting foreign nucleic acids into a cell for the purpose of altering cell properties[253]. Using a nanopore chip, Kurz et al. reported a method of cell transfection where a single cell gene was delivered by electroporation[113]. They designed a multilayer cross-channel PDMS microfluidic device that holds the Si chip with a SiN membrane that contains the nanopore. A top-down microscopy setup was designed for optical integration with this device. It featured a dichroic mirror arrangement to separate the fluorescence signal, and a CCD camera was used to monitor and record the optical events. Fig. 6 (b) depicts the schematic representation of the experimental setup along with other details. In this study, optical tweezers were used for trapping cancer cells in the proximity of the nanopore. At first, they performed a simulation that showed that if the cell membrane was within 10 nm of the SiN membrane then the enhanced electric field (40% voltage drops across the cell membrane) near the nanopore rendered the cell membrane permeable to specific target particles. Based on the simulation results, the cell was reprogrammed by transfecting it with a desired nucleic acid at single molecule resolution. The authors systematically showed how optically labelled nucleic acids were transfecting inside the optically trapped cancer cell and observed that those labelled particles were gradually accumulating near the nucleus. The fluorescence signal had good correspondence with the nanopore translocation count. Interestingly, the translocation direction of the target can be reversed by altering the polarity of the potential applied across the nanopore. In a separate study, this technique was used to detect cell secretion[254].

Recently, the gene editing methodology based on clustered regularly interspaced short palindromic repeats (CRISPR) has been combined with nanopore sensing. CRISPR has been explored widely as genome editing and diagnostic and has become a hot spot of research over the last several years. Most common approaches to deliver the cas9 protein and the guide RNA to a cell of interest are designed based on viral or chemically mediated toxic methods which imposes a significant safety concern[255]. Cao et al. devised a non-toxic approach for the delivery of nucleic acids, functional protein, and Cas9 single-guide RNA based on a nanopore-electroporation platform[114]. The approach is based on a track-etched polycarbonate (PC) water-filter membrane on which an array of ~100 nm nanopores was fabricated. The PC chip was then held and sealed with PDMS holders. A schematic of the experimental setup and nanopore-electroporation principle is depicted in Fig. 6 (c). The cell of interest was cultured overnight on the device and flat titanium electrodes were used to introduce electrical voltage to the device. One remarkable feature of this method is that it facilitates localized electroporation on a nanosized area rather than the conventional electroporation that perforated the whole cell. Using this method, the authors demonstrated a nanopore-electrophoresis mechanism for delivering Cas9 single

guide RNA ribonucleoproteins into both adherent and suspension cells with up to 80% delivery efficiency and >95% cell viability. Additionally, the introduction of the Cas9 ribonucleoproteins allowed them to enable genetic editing of the cells. This is in contrast to conventional methods that require specialized delivery buffer, expensive materials, and a complicated fabrication process, this method offers a low-cost, easy and simple method for intracellular delivery which has the potential to develop into a full-fledged universal method for intracellular manipulation.

4.2.6 Nanopores and plasmons—(Surface) plasmons are collective electronic excitations in metals that have garnered great interest in nanotechnology, nano-optics and nanophotonics because they can be leveraged to dramatically enhance electric fields with nanometer confinement and precision[256,257]. Not surprisingly, this has recently led to the exploration of using plasmonic structures in conjunction with nanopores for improved sensing performance [118,258]. The electric field enhancement depends on the geometry of the plasmonic structure, wavelength and the polarization of the excitation light [259–261]. The integration of nanopores with plasmonic sensors paves the way to detecting the presence of particular targets without surface attachment, and, thus, higher throughput and reusability of the plasmonic sensor by preventing saturation of the sensing volume with target particles[75]. For potential applications, researchers have investigated the integration of nanopores with different plasmonic nanostructures such as bowtie[262], inverted bowtie[110], bullseye[263], and gold nanowells[111]. Moreover, plasmonic nanopores offer different ways of optical signal detection from the target such as fluorescence, scattering light, and Raman scattering [149].

Verschueren et al. reported a plasmonic nanopore based on an inverted bowtie structure that enables label-free detection of biomolecules including DNAs by enhancing the light transmission in the vicinity of the nanopore[110]. Fig. 7 (a) shows the structure of an inverted bowtie plasmonic nanopore with a ~20nm nanopore milled right in the feed gap of the structure where the electric field enhancement is maximum. E-beam lithography was used to fabricate the inverted bowtie structure where, at first, they formed a trilayer stack of polymer on a Si wafer. After patterning the photoresist, a 100 nm gold layer was deposited on to the stacks using e-beam evaporation. The gold flake was then stripped from the substrate by submerging the structure in a 3% KOH solution. The flake was then picked up, placed on a SiN and sealed onto the sample with PDMS. Finally, a nanopore was milled on the feed gap using TEM. The chip was then mounted on a custom-made PEEK flow cell that allows for optical integration. The plasmonic nanopore device was sandwiched between two objectives as shown in Fig. 7 (a). One of them was used for excitation and the other for monitoring the transmission. When a particle passed through the pore, it changed the surrounding dielectric environment and altered the optical transmission at the resonance wavelength. The plasmonic nanopore offers optical translocation signal intensity that is independent of buffer condition and applied voltage. It only depends on how the particle is blocking the optical sensing volume inside the nanopore channel. This approach overcomes some of the limitations of conventional nanopore ionic current sensing, including the high salt concentration requirement and capacitive noise. Therefore, plasmonic nanopores offer high bandwidth data acquisition and high signal to noise ratio at low voltage and low buffer salt concentration where the ionic current is mostly noise dominated.

Most electro-optical analyte detection techniques suffer from the common issue of high photoluminescence background emerging from the nanopore (SiN, SiO_2 etc.) membrane material. Unfortunately, the photoluminescence falls within the fluorescence spectrum, thus degrading the SNR. Assad et al. demonstrated a subwavelength plasmonic nanowell (PNW) based electro-optical detection scheme that enhances the signal strength and improves the SNR[111]. To fabricate the PNW-nanopore device, at first, they created a gold nano well array on the chip and then chemically etched the substrate layer to form a free-standing SiN membrane. Using controlled buffer oxide etching, the SiN layer was further thinned down to 10 nm and finally, nanopores were milled at the center of the nanowells using a TEM. The chip was mounted on a custom CTFE cell using silicone rubber that forms the cis and trans sides of the nanopore. A confocal microscope setup was designed for optical integration which is shown in Fig. 7b (i) and a schematic representation of the cross-section of the PNW-nanopore chip is shown in the zoomed in view. The plasmonic nanowell structure enhances the local electromagnetic field intensity when illuminated by a laser at a particular wavelength (here 660 nm). To verify the device functionality, they electro-optically detected 5 kbp ds-DNAs with high-brightness fluorophores and achieved an order of magnitude enhanced optical signal compared to a standard nanopore chip as depicted in Fig. 7b (ii). Additionally, a sixfold enhancement in event rate was obtained compared to a standard nanopore device. This methodology offers better synchronization between electrical and optical signals as the particles are only excited when they cross the nanopore and reach the optical sensing volume inside the gold cavity.

5 Optofluidic integration

Optofluidics combines integrated photonics and microfluidics in a single platform[101–104]. The microfluidic system provides a native fluidic environment and that facilitates sample processing and preparation, whereas optical methods provide non-invasive imaging, detection and manipulation. One main challenge in designing optofluidic devices is the confinement of light within the low indexed fluidic medium rather than the surrounding high indexed medium. Several methods exist to address this issue such as slot waveguides, Teflon AF waveguides etc.[264]. However, a convenient well-developed approach to address the paradox of guiding light through a low index medium is to use anti-resonant reflective optical waveguide (ARROW). Yin et al. reported the development of a planar ARROW device that is constructed with alternating layers of dielectric materials having a suitable thickness[265]. The ARROW waveguide based optofluidic device has been successfully used to probe and detect single molecules including amplification-free Ebola detection[217], multiplexed detection of single viruses[266], trapping and manipulation of single particles[267–270], diagnostics applications,[271–273]. Thus, integration of nanopores with ARROWs paves the way to incorporate these existing methodologies with nanopores while adding more functionality. The planar geometry overcomes the complex arrangement and painstaking alignment issues of commonly used top-down optical microscopy[205]. However, to take full advantage of optical and fluidic control over particles, planar optofluidic integration is desirable. Liu et al. first reported the integration of optical techniques with nanopore sensing that allows for simultaneous electro-optical detection of single molecules[52]. A schematic representation of this device and electro-optical detection scheme

is depicted in Fig. 8a (i). A nanopore was milled on the LC channel using FIB milling[160]. As shown in the figure, two reservoirs (2 and 3) were attached at the ends of the LC channel while one reservoir (reservoir 1) was placed on top of the milled nanopore and acted as the cis side of the nanopore. A bias voltage was applied across reservoirs 1 and 3 which electrophoretically pulled the analytes from reservoir 1 into the LC channel (trans side in this case) of the device, creating the signatory transient current spike in the current signal. In addition to this electrical detection capability, the device has interconnected SC waveguides that enable light to travel to and from the LC channel. Fiber coupled lasers are typically used to excite fluorescently labeled analytes via the excitation SC waveguide. As the excitation SC waveguide is connected to the LC channel, light is launched into the LC channel, creating a femtoliter excitation volume that is ideal for probing single molecules. As soon as a labeled analyte passes through the excitation spot, it emits fluorescent light at a different wavelength compared to the excitation light. The generated fluorescence signal is then collected via the collection SC waveguide (orthogonal to the excitation SC waveguide as shown in Fig. 8a (i), filtered to discard the excitation light and background noise and finally sent to a sensitive photodetector using connectorized optical fibers. The device uniquely combines microfluidics, optical techniques and nanopore technology in a single platform while offering planar geometry for optical access and additional single molecule manipulation options. To validate the device functionality, the translocated particles were optically detected and a high correlation between the electrical and optical detection spikes was found as both were coming from the same particle. For better visualization, a schematic representation of how the electrical and optical detection is taking place in the device is illustrated in Fig. 8a (ii) and an actual electrical (black) and optical (red) trace of electro-optical detection of single H1N1 influenza virus is shown in Fig. 8a (iii). In addition, different particles contained in a mixture were discriminated based on their electrical detection signatures and optical fluorescence signals which often is difficult to resolve using only one technique (either electrical or optical) due to overlapping subpopulations. Furthermore, the device is sensitive enough to optically detect single DNA molecules as illustrated by the electro-optical detection of single λ-DNA in a separate study by the same group[247]. In addition to nucleic acids a variety of molecules including ribosomes, proteins and celluloses were also detected using a feedback-controlled device that enabled on-demand deliver and detection of single particles[45].

Apart from electro-optical detection, Rahman et al. reported a new approach to improve the performance of nanopore sensing with optofluidic devices by incorporating feedback control and capture enhancement, respectively. Nanopores have large electric fields only within a small range around the pore (capture radius) which is on the order of a few microns[274,275]. Accordingly, nanopores capture only analytes available within that small capture volume in its immediate vicinity. In other words, the nanopore capture process is dominated by the local concentration within a very small capture volume rather than the bulk concentration. This severely hampers the nanopore throughput, event frequency rate (capture rate) and the limit of detection especially, at low concentrations[15,276–278]. Rahman et al. introduced a solution to this problem based on the pre-concentration of molecular targets on microscale carrier beads, followed by optical delivery and trapping of these carrier beads and finally thermally releasing the targets in the vicinity of nanopore, thus enhancing

the local target concentration[95]. The conceptual representation of this methodology, which was dubbed trap assisted capture rate enhancement (TACRE), is depicted in Fig. 8b (i). In this study, target DNAs (corresponding to a melanoma cancer gene) were bound off-chip to functionalized magnetic beads [216,228]. A sample aliquot containing the target carrying magnetic beads (carrier beads) was loaded in either reservoir 1 or 3 as shown in in Fig. 8b (ii). Using pressure driven flow, the carrier beads flowed through the LC channel in a specific direction (inlet to outlet). The carrier beads were then optically collected in a loss-based dual-beam trap first demonstrated by Kühn et al. on a similar optofluidic chip [269]. In a loss-based trap, two counter-propagating optical beams are launched in the LC channel to trap particles at any point along the LC channel where the optical scattering forces on the particle are equal. Remarkably, a loss-based trap facilitates accumulation and trapping of multiple particles[279] which is essential for TACRE. A significant enhancement of the nanopore capture rate was observed by trapping a single carrier bead and releasing the analytes in the proximity of the nanopore, followed by an electrical measurement of nanopore detection. A linear enhancement in capture rate up to two orders of magnitude was observed as more beads were trapped. This methodology has the potential to detect analytes at ultra-low concentrations, and produce quantum leaps in throughput and limits of detection for diagnostics applications at clinically relevant concentrations. Another approach to improve particle delivery to the nanopore was reported by Freedman et al. who used dielectrophoretic trapping of DNAs near the tip of a nanopipette to increase the local DNA concentration at the pore[280]. Chuah et al. demonstrated a method in which antibody-modified magnetic nanoparticles were driven to an array of nanopores with an external magnet. This also improved the nanopore capture rate and limit of detection[281].

Electronic controls probably provide the most efficient, high-speed control of process and machineries both in the laboratory research and industrial applications[282]. Due to the numerous advantages, some researchers incorporated electronic control over nanopores for different control mechanism. Rahman et al. recently reported microcontroller-based control over a nanopore for on-demand delivery of biomolecules with programmable features that added a whole new dimension in nanopore research[45]. The concept was implemented on the optofluidic nanopore platform described above nanopores, but this time with an added feedback control over the nanopore voltage by sensing nanopore current using a microcontroller and a relay. A schematic representation of the feedback-control methodology is shown in Fig. 8c (i). In this study, the nanopore current was fed to a microcontroller input which was continuously monitored and analyzed. The microcontroller was programmed in a way that it could detect a molecular translocation by identifying the translocation spike based on a predetermined threshold. As soon as a translocation was detected, the microcontroller sent a signal to the solid-state relay to disconnect the circuit and turn off the voltage across the nanopore to prevent further translocation. To validate this voltage gating functionality, the authors demonstrated voltage gated delivery of a single ribosome, and the corresponding current and voltage traces are depicted in Fig. 8c (ii). As the system is reconfigurable, the platform can deliberately deliver two, three, or any user defined number of particles for further analysis on an on-demand basis. Additionally, the platform can be programmed for any desired off time (duration for which the voltage across the pore is off) and voltage can be automatically re-applied as per the user’s instruction.

The authors demonstrated successive delivery of single ribosomes which was boosted up to near kHz delivery rate to pave the way for a controlled, high throughput single molecule delivery and analysis platform. Moreover, based on the translocation pattern (dwell time and differential current), the microcontroller can discriminate among different targets going through the pore that produce distinguishable translocation features. Using this approach, voltage gating of λ -DNAs from a mixture of ribosome and λ-DNAs was demonstrated. Ribosomes passing through the pore were recognized but did not activate the voltage gating process as seen in Fig. 8c (iii). This approach may find its application in filtering and separation of biomolecules. Furthermore, as the whole system is designed on an optofluidic device, it facilitates further integration of existing single molecule methods developed on such platform. To demonstrate such integration capability, the authors electro-optically detected a single λ-DNA molecule after voltage gating. This platform may potentially be integrated with their existing trapping methodologies[267] for prolonged analysis of individual biomolecules. With numerous reconfigurable settings, this application shows a high degree of integration that can find ways to perform complex tasks towards lab-on-a-chip applications.

One major challenge of multiplexed particle sensing using nanopores is obtaining target selectivity without altering the nanopore surface chemistry or modifying sample preparation steps. It is very challenging to identify and distinguish particles from a mixture based on the standard scatterplot of dwell time vs differential current due to overlapping subpopulation. Recent developments in machine learning approaches allow researchers to extract useful features from the ambiguous translocation signals to successfully distinguish particles. Using this machine learning approach, Arima et al. devised an approach to distinguish targets from a mixture[122]. Apart from the conventional approach to represent translocation using the dwell time and differential current, they have extracted several more features such as pulse area, onset angle, symmetry, bluntness, and inertia. They have employed their developed algorithm on translocations obtained from five different viruses responsible for respiratory diseases passing through a 300 nm diameter pore and were able to discriminate among them with 99% accuracy. Additionally, they demonstrated excellent separation capability among different strains of the same virus particles (influenza A and B). Therefore, real-time and post processing along with digital signal processing techniques applied on nanopore signals has the potential to offer researchers better insight into the complex translocation process which may find applications in different single molecule approaches. The integration of nanopore sensing with optofluidics has opened new avenues for research and applications, but still faces a few issues and challenges for future exploration. These include selecting device materials that are compatible with both optical functions and nanopore detection, fabrication of smaller nanopores with higher precision, ensuring adequately low electrical noise for nanopore sensing in presence of optical light sources and other elements, and pushing for more complete, full-scale integration. At the same time, this effort has just begun and leaves ample room for expansion, for example by using different optofluidic waveguide types such as slot waveguides [283] or the application of the TACRE principle to on-chip nucleic acid sequencing.

Conclusions

The goal of this review was to provide a comprehensive look at nanopore sensors and the current state of their integration in a lab-on-chip format. Despite a few challenges, such as reproducibility of geometrical shape and electrical properties, solid-state nanopores are the clear choice for this purpose. They can be fabricated using a number of methods, can be adapted for use with a broad range of particle types, and lend themselves most easily for integration with a bigger chip-scale system. Nanopore sensors are by now firmly established as powerful and versatile tools for single molecule sensing and analysis. Fundamental properties, fabrication and integration approaches, and examples for detection and analysis of single biomolecules were presented. Particular attention was given to integration of the nanopore sensing paradigm with other components that take advantage of miniaturization such as multi-channel operation, sample preparation processes, multiplexing and multimodal analysis, in particular in conjunction with optical and photonic techniques. The development of integrated nanopore devices is being fuelled by recent advancements in biological techniques, microfluidics, microelectronics and optical methods. This emerging and expanding class of integrated nanopore devices can be used to understand many complex processes at the molecular level and answer fundamental biological questions that have a clear impact on human health. Examples of exciting directions for fundamental research directions include the combination of nanopore sensors with other precision single molecule methosd such as ABEL traps [284] or plasmonic bow-tie traps [285]. In addition, these capabilities are rapidly finding their way into commercial instruments. Particularly attractive areas to explore for real-world applications are the development of multi-channel, multi-target sensors; the integration of sample handling infrastructure while maintaining high sensitivity nanopore detection; and the incorporation of nanopore sensors with emerging integrated systems for on-chip analysis of molecular products such as nucleic acids, proteins, or exosomes from cells or organoids-on-chip [286].

Acknowledgements

This work was supported by the NIH under grants R01EB028608 and R01EB028608-02S1.

References

1. Xie XS, Choi PJ, Li GW, Nam KL and Lia G, Annu. Rev. Biophys, 2008, 37, 417–444. [PubMed: 18573089]
2. Gilboa T, Garden PM and Cohen L, Anal. Chim. Acta, 2020, 1115, 61–85. [PubMed: 32370870]
3. Milos PM, Expert Rev. Mol. Diagn, 2009, 9, 659–666. [PubMed: 19817551]
4. Ashley EA, Nat. Rev. Genet, 2016, 17, 507–522. [PubMed: 27528417]
5. Jain KK, Expert Rev. Mol. Diagn, 2003, 3, 153–161. [PubMed: 12647993]
6. Deniz AA, Mukhopadhyay S. and Lemke EA, J. R. Soc. Interface, 2008, 5, 15–45. [PubMed: 17519204]
7. Miller H, Zhou Z, Shepherd J, Wollman AJM and Leake MC, Reports Prog. Phys, 2018, 81, 024601.
8. Gooding JJ and Gaus K, Angew. Chemie - Int. Ed, 2016, 55, 11354–11366.
9. Muthukumar M, Plesa C. and Dekker C, Phys. Today, 2015, 68, 40–46.
10. Albrecht T, Annu. Rev. Anal. Chem, 2019, 12, 371–387.
11. Albrecht T, Curr. Opin. Electrochem, 2017, 4, 159–165.

12. Houghtaling J, List J. and Mayer M, Small, 2018, 14.
13. Ying YL, Cao C. and Long YT, Analyst, 2014, 139, 3826–3835. [PubMed: 24991734]
14. Hu R, Tong X. and Zhao Q, Adv. Healthc. Mater, 2020, 9, 2000933.
15. Gu L-Q and Shim JW, Analyst, 2010, 135, 441–451. [PubMed: 20174694]
16. Majd S, Yusko EC, Billeh YN, Macrae MX, Yang J. and Mayer M, Curr. Opin. Biotechnol, 2010, 21, 439–476. [PubMed: 20561776]
17. Emerich DF and Thanos CG, Expert Opin. Biol. Ther, 2003, 3, 655–663. [PubMed: 12831370]
18. Kasianowicz JJ, Brandin E, Branton D. and Deamer DW, Proc. Natl. Acad. Sci. U. S. A, 1996, 93, 13770–3. [PubMed: 8943010]
19. Dekker C, Nat. Nanotechnol, 2007, 2, 209–215. [PubMed: 18654264]
20. Reiner JE, Balijepalli A, Robertson JWF, Campbell J, Suehle J. and Kasianowicz JJ, Chem. Rev, 2012, 112, 6431–6451. [PubMed: 23157510]
21. Meller A, Nivon L. and Branton D, Phys. Rev. Lett, 2001, 86, 3435–3438. [PubMed: 11327989]
22. Bates M, Burns M. and Meller A, Biophys. J, 2003, 84, 2366–2372. [PubMed: 12668445]
23. Graham MD, JALA - J. Assoc. Lab. Autom, 2003, 8, 72–81.
24. Howorka S. and Siwy Z, Chem. Soc. Rev, 2009, 38, 2360–2384. [PubMed: 19623355]
25. Deamer D, Akeson M. and Branton D, Nat. Biotechnol, 2016, 34, 518–524. [PubMed: 27153285]
26. Deamer DW and Branton D, Acc. Chem. Res, 2002, 35, 817–825. [PubMed: 12379134]
27. Meller A. and Branton D, Electrophoresis, 2002, 23, 2583–2591. [PubMed: 12210161]
28. Skinner GM, Van Den Hout M, Broekmans O, Dekker C. and Dekker NH, Nano Lett, 2009, 9, 2953–2960. [PubMed: 19537802]
29. Kim Y-R, Li CM, Wang Q. and Chen P, Detecting translocation of individual single stranded DNA homopolymers through a fabricated nanopore chip, 2007, vol. 12.
30. Kowalczyk SW, Tuijtel MW, Donkers SP and Dekker C, Nano Lett, 2010, 10, 1414–1420. [PubMed: 20235508]
31. Harrell CC, Choi Y, Home LP, Baker LA, Siwy ZS and Martin CR, Langmuir, 2006, 22, 10837–10843. [PubMed: 17129068]
32. Fologea D, Gershow M, Ledden B, McNabb DS, Golovchenko JA and Li J, Nano Lett, 2005, 5, 1905–1909. [PubMed: 16218707]
33. Akahori R, Haga T, Hatano T, Yanagi I, Ohura T, Hamamura H, Iwasaki T, Yokoi T. and Anazawa T, Nanotechnology, DOI:10.1088/0957-4484/25/27/275501.
34. Chien CC, Shekar S, Niedzwiecki DJ, Shepard KL and Drndić M, ACS Nano, 2019, 13, 10545–10554. [PubMed: 31449393]
35. Kumar Sharma R, Agrawal I, Dai L, Doyle PS and Garaj S, Nat. Commun, 2019, 10, 4473. [PubMed: 31578328]
36. Plesa C, Verschueren D, Pud S, Van Der Torre J, Ruitenberg JW, Witteveen MJ, Jonsson MP, Grosberg AY, Rabin Y. and Dekker C, Nat. Nanotechnol, 2016, 11, 1093–1097. [PubMed: 27525473]
37. Li J, Gershow M, Stein D, Brandin E. and Golovchenko JA, Nat. Mater, 2003, 2, 611–615. [PubMed: 12942073]
38. Li J. and Talaga DS, J. Phys. Condens. Matter, 2010, 22, 454129. [PubMed: 21339615]
39. Smeets RMM, Kowalczyk SW, Hall AR, Dekker NH and Dekker C, Nano Lett, 2009, 9, 3089–3095. [PubMed: 19053490]
40. Chang H, Kosari F, Andreadakis G, Alam MA, Vasmatzis G. and Bashir R, Nano Lett, 2004, 4, 1551–1556.
41. Shasha C, Henley RY, Stoloff DH, Rynearson KD, Hermann T. and Wanunu M, ACS Nano, 2014, 8, 6425–6430. [PubMed: 24861167]
42. Garalde DR, Snell EA, Jachimowicz D, Sipos B, Lloyd JH, Bruce M, Pantic N, Admassu T, James P, Warland A, Jordan M, Ciccone J, Serra S, Keenan J, Martin S, McNeill L, Wallace EJ, Jayasinghe L, Wright C, Blasco J, Young S, Brocklebank D, Juul S, Clarke J, Heron AJ and Turner DJ, Nat. Methods, 2018, 15, 201–206. [PubMed: 29334379]

43. Van Den Hout M, Skinner GM, Klijnhout S, Krudde V. and Dekker NH, Small, 2011, 7, 2217–2224. [PubMed: 21638785]
44. Wanunu M, Bhattacharya S, Xie Y, Tor Y, Aksimentiev A. and Drndic M, ACS Nano, 2011, 5, 9345–9353. [PubMed: 22067050]
45. Rahman M, Stott MA, Harrington M, Li Y, Sampad MJN, Lancaster L, Yuzvinsky TD, Noller HF, Hawkins AR and Schmidt H, Nat. Commun, 2019, 10, 3712. [PubMed: 31420559]
46. Wei R, Gatterdam V, Wieneke R, Tampé R. and Rant U, Nat. Nanotechnol, 2012, 7, 257–263. [PubMed: 22406921]
47. Yusko EC, Bruhn BR, Eggenberger OM, Houghtaling J, Rollings RC, Walsh NC, Nandivada S, Pindrus M, Hall AR, Sept D, Li J, Kalonia DS and Mayer M, Nat. Nanotechnol, 2017, 12, 360–367. [PubMed: 27992411]
48. Li W, Bell NAW, Hernández-Ainsa S, Thacker VV, Thackray AM, Bujdoso R. and Keyser UF, ACS Nano, 2013, 7, 4129–4134. [PubMed: 23607870]
49. Varongchayakul N, Song J, Meller A. and Grinstaff MW, Chem. Soc. Rev, 2018, 47, 8512–8524. [PubMed: 30328860]
50. Rudenko MI, Holmes MR, Ermolenko DN, Lunt EJ, Gerhardt S, Noller HF, Deamer DW, Hawkins A. and Schmidt H, Biosens. Bioelectron, 2011, 29, 34–39. [PubMed: 21855314]
51. Raveendran M, Leach AR, Hopes T, Aspden JL and Actis P, ACS Sensors, 2020, 5, 3533–3539. [PubMed: 33111519]
52. Liu S, Zhao Y, Parks JW, Deamer DW, Hawkins AR and Schmidt H, Nano Lett, 2014, 14, 4816–4820. [PubMed: 25006747]
53. McMullen A, De Haan HW, Tang JX and Stein D, Nat. Commun, 2014, 5, 4171. [PubMed: 24932700]
54. Sutherland TC, Long YT, Stefureac RI, Bediako-Amoa I, Kraatz HB and Lee JS, Nano Lett, 2004, 4, 1273–1277.
55. Chavis AE, Brady KT, Hatmaker GA, Angevine CE, Kothalawala N, Dass A, Robertson JWF and Reiner JE, ACS Sensors, 2017, 2, 1319–1328. [PubMed: 28812356]
56. Li S, Cao C, Yang J. and Long YT, ChemElectroChem, 2019, 6, 126–129.
57. Fennouri A, Przybylski C, Pastoriza-Gallego M, Bacri L, Auvray L. and Daniel R, ACS Nano, 2012, 6, 9672–9678. [PubMed: 23046010]
58. Liu L, You Y, Zhou K, Guo B, Cao Z, Zhao Y. and Wu H, Angew. Chemie Int. Ed, 2019, 58, 14929–14934.
59. Kukwikila M. and Howorka S, Anal. Chem, 2015, 87, 9149–9154. [PubMed: 26305576]
60. Bell NAW and Keyser UF, J. Am. Chem. Soc, 2015, 137, 2035–2041. [PubMed: 25621373]
61. Celaya G, Perales-Calvo J, Muga A, Moro F. and Rodriguez-Larrea D, ACS Nano, 2017, 11, 5815–5825. [PubMed: 28530800]
62. Plesa C, Ruitenberg JW, Witteveen MJ and Dekker C, Nano Lett, 2015, 15, 3153–3158. [PubMed: 25928590]
63. Bell NAW and Keyser UF, Nat. Nanotechnol, 2016, 11, 645–651. [PubMed: 27043197]
64. Astier Y, Uzun O. and Stellacci F, Small, 2009, 5, 1273–1278. [PubMed: 19242940]
65. German SR, Luo L, White HS and Mega TL, J. Phys. Chem. C, 2013, 117, 703–711.
66. Prabhu AS, Jubery TZN, Freedman KJ, Mulero R, Dutta P. and Kim MJ, J. Phys. Condens. Matter, 2010, 22, 454107. [PubMed: 21339595]
67. Lan WJ, Holden DA, Zhang B. and White HS, Anal. Chem, 2011, 83, 3840–3847. [PubMed: 21495727]
68. Liu L, Kong J, Xie X, Wu H, Ye X, Zhao Z, Wang L. and Liu Q, Chinese Sci. Bull, 2014, 59, 598–605.
69. Ivanov AP, Actis P, Jönsson P, Klenerman D, Korchev Y. and Edel JB, ACS Nano, 2015, 9, 3587–3595. [PubMed: 25794527]
70. Trick JL, Song C, Wallace EJ and Sansom MSP, ACS Nano, 2017, 11, 1840–1847. [PubMed: 28141923]
71. Smirnov SN, Vlassiouk IV and Lavrik NV, ACS Nano, 2011, 5, 7453–7461. [PubMed: 21838311]

72. Gershow M. and Golovchenko JA, Nat. Nanotechnol, 2007, 2, 775–779. [PubMed: 18654430]
73. Liu X, Skanata MM and Stein D, Nat. Commun, 2015, 6, 6222. [PubMed: 25648853]
74. Bell NAW, Chen K, Ghosal S, Ricci M. and Keyser UF, Nat. Commun, 2017, 8, 380. [PubMed: 28855527]
75. Shi X, Verschueren DV and Dekker C, Nano Lett, 2018, 18, 8003–8010. [PubMed: 30460853]
76. Bush J, Maulbetsch W, Lepoitevin M, Wiener B, Mihovilovic Skanata M, Moon W, Pruitt C. and Stein D, Rev. Sci. Instrum, 2017, 88, 113307. [PubMed: 29195372]
77. Robertson JWF, Rodrigues CG, Stanford VM, Rubinson KA, Krasilnikov OV and Kasianowicz JJ, Proc. Natl. Acad. Sci. U. S. A, 2007, 104, 8207–8211. [PubMed: 17494764]
78. Tsutsui M, Yokota K, Arima A, He Y. and Kawai T, ACS Sensors, 2019, 4, 2974–2979. [PubMed: 31576750]
79. Feng J, Graf M, Liu K, Ovchinnikov D, Dumcenco D, Heiranian M, Nandigana V, Aluru NR, Kis A. and Radenovic A, Nature, 2016, 536, 197–200. [PubMed: 27409806]
80. Guo W, Cao L, Xia J, Nie FQ, Wen M, Xue J, Song Y, Zhu D, Wang Y. and Jiang L, Adv. Funct. Mater, 2010, 20, 1339–1344.
81. Wen L, Hou X, Tian Y, Zhai J. and Jiang L, Adv. Funct. Mater, 2010, 20, 2636–2642.
82. Yamazaki H, Hu R, Henley RY, Halman J, Afonin KA, Yu D, Zhao Q. and Wanunu M, Nano Lett, 2017, 17, 7067–7074. [PubMed: 28975798]
83. Shi W, Friedman AK and Baker LA, Anal. Chem, 2017, 89, 157–188. [PubMed: 28105845]
84. Moerner WE and Fromm DP, Rev. Sci. Instrum, 2003, 74, 3597–3619.
85. Walt DR, Anal. Chem, 2013, 85, 1258–1263. [PubMed: 23215010]
86. Nichols RJ and Higgins SJ, Annu. Rev. Anal. Chem, 2015, 8, 389–417.
87. Gu C, Jia C. and Guo X, Small Methods, 2017, 1, 1700071.
88. Walter NG, Huang CY, Manzo AJ and Sobhy MA, Nat. Methods, 2008, 5, 475–489. [PubMed: 18511916]
89. Moerner WE, Proc. Natl. Acad. Sci. U. S. A, 2007, 104, 12596–12602. [PubMed: 17664434]
90. Yanagi I, Akahori R, Aoki M, Harada K. and Takeda KI, Lab Chip, 2016, 16, 3340–3350. [PubMed: 27440476]
91. Varongchayakul N, Hersey JS, Squires A, Meller A. and Grinstaff MW, Adv. Funct. Mater, 2018, 28, 1804182. [PubMed: 31632230]
92. Spitzberg JD, Van Kooten XF, Bercovici M. and Meller A, Nanoscale, 2020, 12, 17805–17811. [PubMed: 32820758]
93. Roman J, Français O, Jarroux N, Patriarche G, Pelta J, Bacri L. and Le Pioufle B, ACS Sensors, 2018, 3, 2129–2137. [PubMed: 30284814]
94. Fu J, Wu L, Qiao Y, Tu J. and Lu Z, Micromachines, 2020, 11, 332.
95. Rahman M, Harrington M, Stott MA, Li Y, Sampad MJN, Yuzvinsky TD, Hawkins AR and Schmidt H, Optica, 2019, 6, 1130. [PubMed: 33598506]
96. Tahvildari R, Beamish E, Briggs K, Chagnon-Lessard S, Sohi AN, Han S, Watts B, Tabard-Cossa V. and Godin M, Small, 2017, 13, 1602601.
97. Tahvildari R, Beamish E, Tabard-Cossa V. and Godin M, Lab Chip, 2015, 15, 1407–1411. [PubMed: 25631885]
98. Rosenstein JK, Wanunu M, Merchant CA, Drndic M. and Shepard KL, Nat. Methods, 2012, 9, 487–492. [PubMed: 22426489]
99. Parsnejad S. and Mason AJ, in CMOS Circuits for Biological Sensing and Processing, Springer International Publishing, Cham, 2017, pp. 1–21.
100. Magierowski S, Huang Y, Wang C. and Ghafar-Zadeh E, Biosensors, 2016, 6, 42.
101. Psaltis D, Quake SR and Yang C, Nature, 2006, 442, 381–386. [PubMed: 16871205]
102. Minzioni P, Osellame R, Sada C, Zhao S, Omenetto FG, Gylfason KB, Haraldsson T, Zhang Y, Ozcan A, Wax A, Mugele F, Schmidt H, Testa G, Bernini R, Guck J, Liberale C, Berg-Sørensen K, Chen J, Pollnau M, Xiong S, Liu AQ, Shiue CC, Fan SK, Erickson D. and Sinton D, J. Opt. (United Kingdom), 2017, 19, 093003.
103. Monat C, Domachuk P. and Eggleton BJ, Nat. Photonics, 2007, 1, 106–114.

104. Schmidt H. and Hawkins AR, Nat. Photonics, 2011, 5, 598–604.
105. Fan X. and White IM, Nat. Photonics, 2011, 5, 591–597. [PubMed: 22059090]
106. Angeli E, Volpe A, Fanzio P, Repetto L, Firpo G, Guida P, Lo Savio R, Wanunu M. and Valbusa U, Nano Lett, 2015, 15, 5696–5701. [PubMed: 26225640]
107. Pitchford WH, Kim H-J, Ivanov AP, Kim H-M, Yu J-S, Leatherbarrow RJ, Albrecht T, Kim K-B and Edel JB, ACS Nano, 2015, 9, 1740–1748. [PubMed: 25635821]
108. Shi X, Gao R, Ying Y-L, Si W, Chen Y. and Long Y-T, Faraday Discuss, 2015, 184, 85–99. [PubMed: 26420730]
109. Lu W, Hu R, Tong X, Yu D. and Zhao Q, Small Struct, 2020, 1, 2000003.
110. Verschueren DV, Pud S, Shi X, De Angelis L, Kuipers L. and Dekker C, ACS Nano, 2019, 13, 61–70. [PubMed: 30512931]
111. Assad ON, Gilboa T, Spitzberg J, Juhasz M, Weinhold E. and Meller A, Adv. Mater, 2017, 29, 1605442.
112. Ivankin A, Henley RY, Larkin J, Carson S, Toscano ML and Wanunu M, ACS Nano, 2014, 8, 10774–10781. [PubMed: 25232895]
113. Kurz V, Tanaka T. and Timp G, Nano Lett, 2014, 14, 604–611. [PubMed: 24471806]
114. Cao Y, Ma E, Cestellos-Blanco S, Zhang B, Qiu R, Su Y, Doudna JA and Yang P, Proc. Natl. Acad. Sci, 2019, 116, 7899–7904. [PubMed: 30923112]
115. Spiering A, Getfert S, Sischka A, Reimann P. and Anselmetti D, Nano Lett, 2011, 11, 2978–2982. [PubMed: 21667921]
116. Van Den Hout M, Vilfan ID, Hage S. and Dekker NH, Nano Lett, 2010, 10, 701–707. [PubMed: 20050676]
117. Keyser UF, Van Der Does J, Dekker C. and Dekker NH, in Review of Scientific Instruments, 2006, vol. 77, p. 105105.
118. Garoli D, Yamazaki H, MacCaferri N. and Wanunu M, Nano Lett, 2019, 19, 7553–7562. [PubMed: 31587559]
119. Smeets RMM, Keyser UF, Krapf D, Wu M-Y, Dekker NH and Dekker C, Nano Lett, 2006, 6, 89–95. [PubMed: 16402793]
120. Kowalczyk SW and Dekker C, Nano Lett, 2012, 12, 4159–4163. [PubMed: 22803839]
121. Wanunu M, Dadosh T, Ray V, Jin J, McReynolds L. and Drndić M, Nat. Nanotechnol, 2010, 5, 807–814. [PubMed: 20972437]
122. Arima A, Tsutsui M, Yoshida T, Tatematsu K, Yamazaki T, Yokota K, Kuroda S, Washio T, Baba Y. and Kawai T, ACS Sensors, 2020, 5, 3398–3403. [PubMed: 32933253]
123. Ashkenasy N, Sánchez-Quesada J, Bayley H. and Ghadiri MR, Angew. Chemie, 2005, 117, 1425–1428.
124. Deamer DW and Akeson M, Trends Biotechnol, 2000, 18, 147–151. [PubMed: 10740260]
125. Bayley H, Clin. Chem, 2015, 61, 25–31. [PubMed: 25477535]
126. Goto Y, Akahori R, Yanagi I. and Takeda K, J. Hum. Genet, 2019, 1–9. [PubMed: 30390021]
127. Wasfi A, Awwad F. and Ayesh AI, Biosens. Bioelectron, 2018, 119, 191–203. [PubMed: 30125881]
128. Jain M, Olsen HE, Paten B. and Akeson M, Genome Biol, 2016, 17, 239. [PubMed: 27887629]
129. Wanunu M, Phys. Life Rev, 2012, 9, 125–158. [PubMed: 22658507]
130. Song L, Hobaugh MR, Shustak C, Cheley S, Bayley H. and Gouaux JE, Science (80-.)., 1996, 274, 1859–1866.
131. Butler TZ, Pavlenok M, Derrington IM, Niederweis M. and Gundlach JH, Proc. Natl. Acad. Sci. U. S. A, 2008, 105, 20647–20652. [PubMed: 19098105]
132. Stefureac R, Long YT, Kraatz HB, Howard P. and Lee JS, Biochemistry, 2006, 45, 9172–9179. [PubMed: 16866363]
133. Soskine M, Biesemans A, Moeyaert B, Cheley S, Bayley H. and Maglia G, Nano Lett, 2012, 12, 4895–4900. [PubMed: 22849517]
134. Mohammad MM, Howard KR and Movileanu L, J. Biol. Chem, 2011, 286, 8000–8013. [PubMed: 21189254]

135. Zhuang T. and Tamm LK, Angew. Chemie, 2014, 126, 6007–6012.
136. Chimerel C, Movileanu L, Pezeshki S, Winterhalter M. and Kleinekathöfer U, Eur. Biophys. J, 2008, 38, 121–125. [PubMed: 18726094]
137. Goyal P, Krasteva PV, Van Gerven N, Gubellini F, Van Den Broeck I, Troupiotis-Tsaïlaki A, Jonckheere W, Péhau-Arnaudet G, Pinkner JS, Chapman MR, Hultgren SJ, Howorka S, Fronzes R. and Remaut H, Nature, 2014, 516, 250–253. [PubMed: 25219853]
138. Wendell D, Jing P, Geng J, Subramaniam V, Lee TJ, Montemagno C. and Guo P, Nat. Nanotechnol, 2009, 4, 765–772. [PubMed: 19893523]
139. Wang S, Ji Z, Yan E, Haque F. and Guo P, Virology, 2017, 500, 285–291. [PubMed: 27181501]
140. Zhou Z, Ji Z, Wang S, Haque F. and Guo P, Biomaterials, 2016, 105, 222–227. [PubMed: 27529454]
141. Rhee M. and Burns MA, Trends Biotechnol, 2007, 25, 174–181. [PubMed: 17320228]
142. Akeson M, Branton D, Kasianowicz JJ, Brandin E. and Deamer DW, Biophys. J, 1999, 77, 3227–3233. [PubMed: 10585944]
143. Jain M, Fiddes IT, Miga KH, Olsen HE, Paten B. and Akeson M, Nat. Methods, 2015, 12, 351–356. [PubMed: 25686389]
144. Wang S, Zhao Z, Haque F. and Guo P, Curr. Opin. Biotechnol, 2018, 51, 80–89. [PubMed: 29232619]
145. Chen Q. and Liu Z, Sensors (Switzerland), 2019, 19.
146. Li J, Stein D, McMullan C, Branton D, Aziz MJ and Golovchenko JA, Nature, 2001, 412, 166–169. [PubMed: 11449268]
147. Lee K, Park K-B, Kim H-J, Yu J-S, Chae H, Kim H-M and Kim K-B, Adv. Mater, 2018, 30, 1704680.
148. Wu GS, Zhang Y, Si W, Sha JJ, Liu L. and Chen YF, Sci. China Technol. Sci, 2014, 57, 1925–1935.
149. Xue L, Yamazaki H, Ren R, Wanunu M, Ivanov AP and Edel JB, Nat. Rev. Mater, 2020, 5, 931–951.
150. Nehra A, Ahlawat S. and Singh KP, Sensors Actuators, B Chem, 2019, 284, 595–622.
151. Han A, Creus M, Schürmann G, Linder V, Ward TR, De Rooij NF and Staufer U, Anal. Chem, 2008, 80, 4651–4658. [PubMed: 18470996]
152. Hall AR, Scott A, Rotem D, Mehta KK, Bayley H. and Dekker C, Nat. Nanotechnol, 2010, 5, 874–877. [PubMed: 21113160]
153. Cressiot B, Greive SJ, Mojtabavi M, Antson AA and Wanunu M, Nat. Commun, 2018, 9, 1–7. [PubMed: 29317637]
154. Bell NAW, Engst CR, Ablay M, Divitini G, Ducati C, Liedl T. and Keyser UF, Nano Lett, 2012, 12, 512–517. [PubMed: 22196850]
155. Bell NAW and Keyser UF, FEBS Lett, 2014, 588, 3564–3570. [PubMed: 24928438]
156. Wang Z, Liu Y, Yu L, Li Y, Qian G. and Chang S, Analyst, 2019, 144, 5037–5047. [PubMed: 31290857]
157. Kudr J, Skalickova S, Nejdl L, Moulick A, Ruttkay-Nedecky B, Adam V. and Kizek R, Electrophoresis, 2015, 36, 2367–2379. [PubMed: 26046318]
158. Stein D, Li J. and Golovchenko JA, Phys. Rev. Lett, 2002, 89, 276106. [PubMed: 12513225]
159. Stein DM, McMullan CJ, Li J. and Golovchenko JA, Rev. Sci. Instrum, 2004, 75, 900–905.
160. Liu S, Yuzvinsky TD and Schmidt H, ACS Nano, 2013, 7, 5621–5627. [PubMed: 23697604]
161. Deng T, Li M, Wang Y. and Liu Z, Sci. Bull, 2015, 60, 304–319.
162. Marshall MM, Yang J. and Hall AR, Scanning, 2012, 34, 101–106. [PubMed: 22331671]
163. Yang J, Ferranti DC, Stern LA, Sanford CA, Huang J, Ren Z, Qin LC and Hall AR, Nanotechnology, DOI:10.1088/0957-4484/22/28/285310.
164. Spinney PS, Howitt DG, Smith RL and Collins SD, Nanotechnology, DOI:10.1088/0957-4484/21/37/375301.
165. Kim MJ, McNally B, Murata K. and Meller A, Nanotechnology, 2007, 18.

166. Zandbergen HW, Van Duuren RJHA, Alkemade PFA, Lientschnig G, Vasquez O, Dekker G. and Tichelaar FD, Nano Lett, 2005, 5, 549–553. [PubMed: 15755112]
167. Chang H, Iqbal SM, Stach EA, King AH, Zaluzec NJ and Bashir R, Appl. Phys. Lett, 2006, 88, 103109.
168. Kim MJ, Wanunu M, Bell DC and Meller A, Adv. Mater, 2006, 18, 3149–3153.
169. Storm AJ, Chen JH, Ling XS, Zandbergen HW and Dekker C, Nat. Mater, 2003, 2, 537–540. [PubMed: 12858166]
170. Kennedy E, Dong Z, Tennant C. and Timp G, Nat. Nanotechnol, 2016, 11, 968–976. [PubMed: 27454878]
171. Kolmogorov M, Kennedy E, Dong Z, Timp G. and Pevzner PA, PLOS Comput. Biol, 2017, 13, e1005356. [PubMed: 28486472]
172. Kwok H, Briggs K. and Tabard-Cossa V, PLoS One, 2014, 9, e92880. [PubMed: 24658537]
173. Waugh M, Briggs K, Gunn D, Gibeault M, King S, Ingram Q, Jimenez AM, Berryman S, Lomovtsev D, Andrzejewski L. and Tabard-Cossa V, Nat. Protoc, 2020, 15, 122–143. [PubMed: 31836867]
174. Yanagi I, Akahori R, Hatano T. and Takeda KI, Sci. Rep, 2014, 4, 1–7.
175. Yin B, Fang S, Zhou D, Liang L, Wang L, Wang Z, Wang D. and Yuan J, ACS Appl. Bio Mater, 2020, 3, 6368–6375.
176. Yanagi I, Akahori R. and ichi Takeda K, Sci. Rep, 2019, 9, 13143. [PubMed: 31511597]
177. Dittrich PS and Manz A, Nat. Rev. Drug Discov, 2006, 5, 210–218. [PubMed: 16518374]
178. Briggs K, Charron M, Kwok H, Le T, Chahal S, Bustamante J, Waugh M. and Tabard-Cossa V, Nanotechnology, DOI:10.1088/0957-4484/26/8/084004.
179. Goto Y, Yanagi I, Matsui K, Yokoi T. and Takeda KI, Sci. Rep, 2016, 6, 31324. [PubMed: 27499264]
180. Bello J. and Shim J, Biomed. Microdevices, 2018, 20, 38. [PubMed: 29680876]
181. Karhanek M, Kemp JT, Pourmand N, Davis RW and Webb CD, Nano Lett, 2005, 5, 403–407. [PubMed: 15794633]
182. Yu RJ, Ying YL, Gao R. and Long YT, Angew. Chemie - Int. Ed, 2019, 58, 3706–3714.
183. Lin X, Ivanov AP and Edel JB, Chem. Sci, 2017, 8, 3905–3912. [PubMed: 28626560]
184. Sha J, Ni Z, Liu L, Yi H. and Chen Y, Nanotechnology, DOI:10.1088/0957-4484/22/17/175304.
185. Freedman JR, Mattia D, Korneva G, Gogotsi Y, Friedman G. and Fontecchio AK, Appl. Phys. Lett, 2007, 90, 103108.
186. Han H, Huang Z. and Lee W, Nano Today, 2014, 9, 271–304.
187. Park SR, Peng H. and Ling XS, Small, 2007, 3, 116–119. [PubMed: 17294481]
188. Deng T, Li M, Chen J, Wang Y. and Liu Z, J. Phys. Chem. C, 2014, 118, 18110–18115.
189. Deng T, Chen J, Si W, Yin M, Ma W. and Liu Z, J. Vac. Sci. Technol. B, Nanotechnol. Microelectron. Mater. Process. Meas. Phenom, 2012, 30, 061804.
190. Siwy Z. and Fuliński A, Phys. Rev. Lett, 2002, 89, 198103. [PubMed: 12443155]
191. Apel PY, Blonskaya IV, Dmitriev SN, Orelovitch OL, Presz A. and Sartowska BA, Nanotechnology, DOI:10.1088/0957-4484/18/30/305302.
192. Wharton JE, Jin P, Sexton LT, Horne LP, Sherrill SA, Mino WK and Martin CR, Small, 2007, 3, 1424–1430. [PubMed: 17615589]
193. Ma T, Janot JM and Balme S, Small Methods, 2020, 4, 2000366.
194. Daw R. and Finkelstein J, Nature, 2006, 442, 367.
195. Craighead H, Nature, 2006, 442, 387–393. [PubMed: 16871206]
196. Azizipour N, Avazpour R, Rosenzweig DH, Sawan M. and Ajji A, Micromachines, 2020, 11, 1–15.
197. Miller EM and Wheeler AR, Anal. Bioanal. Chem, 2009, 393, 419–426. [PubMed: 18820902]
198. Berlanda SF, Breitfeld M, Dietsche CL and Dittrich PS, Anal. Chem, 2020, 93, 311–331. [PubMed: 33170661]
199. Khandurina J. and Guttman A, J. Chromatogr. A, 2002, 943, 159–183. [PubMed: 11833638]

200. Holmes D. and Gawad S, Humana Press, Totowa, NJ, 2010, pp. 55–80.
201. Weibel DB and Whitesides GM, Curr. Opin. Chem. Biol, 2006, 10, 584–591. [PubMed: 17056296]
202. Whitesides GM, Nature, 2006, 442, 368–373. [PubMed: 16871203]
203. Su F, Chakrabarty K. and Fair RB, IEEE Trans. Comput. Des. Integr. Circuits Syst, 2006, 25, 211–223.
204. Watson C. and Senyo S, HardwareX, 2019, 5, e00063. [PubMed: 31192312]
205. Liu S, Hawkins AR and Schmidt H, Microchim. Acta, 2016, 183, 1275–1287.
206. Kumar S, Wittenberg NJ and Oh SH, Anal. Chem, 2013, 85, 971–977. [PubMed: 23214989]
207. Raj M K. and Chakraborty S, J. Appl. Polym. Sci, 2020, 137, 48958.
208. Jiang Y, Wang H, Li S. and Wen W, Sensors (Switzerland), 2014, 14, 6952–6964.
209. Chen C, Mehl BT, Munshi AS, Townsend AD, Spence DM and Martin RS, Anal. Methods, 2016, 8, 6005–6012. [PubMed: 27617038]
210. Kuo TC, Cannon DM, Chen Y, Tulock JJ, Shannon MA, Sweedler JV and Bohn PW, Anal. Chem, 2003, 75, 1861–1867. [PubMed: 12713044]
211. Zhou K, Kovarik ML and Jacobson SC, J. Am. Chem. Soc, 2008, 130, 8614–8616. [PubMed: 18549214]
212. Jain T, Guerrero RJS, Aguilar CA and Karnik R, Anal. Chem, 2013, 85, 3871–3878. [PubMed: 23347165]
213. Holmes MR, Shang T, Hawkins AR, Rudenko M, Measor P. and Schmidt H, J. Micro. Nanolithogr. MEMS. MOEMS, 2010, 9, 23004. [PubMed: 21922035]
214. Parks JW, Cai H, Zempoaltecatl L, Yuzvinsky TD, Leake K, Hawkins AR and Schmidt H, Lab Chip, 2013, 13, 4118. [PubMed: 23969694]
215. Parks JW, Olson MA, Kim J, Ozcelik D, Cai H, Carrion R, Patterson JL, Mathies RA, Hawkins AR and Schmidt H, Biomicrofluidics, 2014, 8, 054111. [PubMed: 25584111]
216. Cai H, Stott MA, Ozcelik D, Parks JW, Hawkins AR and Schmidt H, Biomicrofluidics, 2016, 10, 064116. [PubMed: 28058082]
217. Cai H, Parks JW, Wall TA, Stott MA, Stambaugh A, Alfson K, Griffiths A, Mathies RA, Carrion R, Patterson JL, Hawkins AR and Schmidt H, Sci. Rep, 2015, 5, 14494. [PubMed: 26404403]
218. Uddin A, Yemenicioglu S, Chen C-H, Corgliano E, Milaninia K, Xia F, Plaxco K. and Theogarajan L, Biosensing Nanomedicine V, 2012, 8460, 846010.
219. Nanopore Sequencing, https://sequencing.roche.com/en/science-education/technology/nanopore-sequencing.html, (accessed 13 March 2021).
220. Liao Z, Zhang Y, Li Y, Miao Y, Gao S, Lin F, Deng Y. and Geng L, Biosens. Bioelectron, 2019, 126, 697–706. [PubMed: 30544083]
221. Rajapaksha RDAA, Azman NAN, Uda MNA, Hashim U, Gopinath SCB and Fernando CAN, in AIP Conference Proceedings, American Institute of Physics Inc., 2018, vol. 2045, p. 020020.
222. Bell NAW, Thacker VV, Hernández-Ainsa S, Fuentes-Perez ME, Moreno-Herrero F, Liedl T. and Keyser UF, Lab Chip, 2013, 13, 1859–1862. [PubMed: 23563625]
223. Zeng S, Wen C, Zhang SL and Zhang Z, IEEE Sens. J, 2020, 20, 1558–1563.
224. Gong X, Patil AV, Ivanov AP, Kong Q, Gibb T, Dogan F, Demello AJ and Edel JB, Anal. Chem, 2014, 86, 835–841. [PubMed: 24328180]
225. Tetala KKR and Vijayalakshmi MA, Anal. Chim. Acta, 2016, 906, 7–21. [PubMed: 26772122]
226. Yeo LY, Chang HC, Chan PPY and Friend JR, Small, 2011, 7, 12–48. [PubMed: 21072867]
227. Sahore V, Sonker M, Nielsen AV, Knob R, Kumar S. and Woolley AT, Anal. Bioanal. Chem, 2018, 410, 933–941. [PubMed: 28799040]
228. Parks JW, Olson MA, Kim J, Ozcelik D, Cai H, Carrion R, Patterson JL, Mathies RA, Hawkins AR and Schmidt H, Biomicrofluidics, 2014, 8, 054111. [PubMed: 25584111]
229. Velasco-Garcia MN, Semin. Cell Dev. Biol, 2009, 20, 27–33. [PubMed: 19429488]
230. Spackova B, Wrobel P, Bockova M. and Homola J, Proc. IEEE, 2016, 104, 2380–2408.
231. Leung A, Shankar PM and Mutharasan R, Sensors Actuators B Chem, 2007, 125, 688–703.
232. Juan ML, Righini M. and Quidant R, Nat. Photonics, 2011, 5, 349–356.

233. Moffitt JR, Chemla YR, Smith SB and Bustamante C, Annu. Rev. Biochem, 2008, 77, 205–228. [PubMed: 18307407]
234. Tan H, Hu H, Huang L. and Qian K, Analyst, 2020, 145, 5699–5712. [PubMed: 32692343]
235. Gilboa T. and Meller A, Analyst, 2015, 140, 4733–4747. [PubMed: 25684652]
236. Branton D, Deamer DW, Marziali A, Bayley H, Benner SA, Butler T, Di Ventra M, Garaj S, Hibbs A, Huang X, Jovanovich SB, Krstic PS, Lindsay S, Ling XS, Mastrangelo CH, Meller A, Oliver JS, V Pershin Y, Ramsey JM, Riehn R, V Soni G, Tabard-Cossa V, Wanunu M, Wiggin M. and Schloss JA, Nat. Biotechnol, 2008, 26, 1146–1153. [PubMed: 18846088]
237. Luan B, Stolovitzky G. and Martyna G, Nanoscale, 2012, 4, 1068–1077. [PubMed: 22081018]
238. Yuan Z, Liu Y, Dai M, Yi X. and Wang C, Nanoscale Res. Lett, 2020, 15. [PubMed: 31950368]
239. Liu Z, Wang Y, Deng T. and Chen Q, J. Nanomater, 2016, 2016, 1–13.
240. Fologea D, Uplinger J, Thomas B, McNabb DS and Li J, Nano Lett, 2005, 5, 1734–1737. [PubMed: 16159215]
241. Kowalczyk SW, Wells DB, Aksimentiev A. and Dekker C, Nano Lett, 2012, 12, 1038–1044. [PubMed: 22229707]
242. Di Fiori N, Squires A, Bar D, Gilboa T, Moustakas TD and Meller A, Nat. Nanotechnol, 2013, 8, 946–951. [PubMed: 24185943]
243. Jain M, Koren S, Miga KH, Quick J, Rand AC, Sasani TA, Tyson JR, Beggs AD, Dilthey AT, Fiddes IT, Malla S, Marriott H, Nieto T, O'Grady J, Olsen HE, Pedersen BS, Rhie A, Richardson H, Quinlan AR, Snutch TP, Tee L, Paten B, Phillippy AM, Simpson JT, Loman NJ and Loose M, Nat. Biotechnol, 2018, 36, 338–345. [PubMed: 29431738]
244. Magi A, Semeraro R, Mingrino A, Giusti B. and D'Aurizio R, Brief. Bioinform, 2017, 19, 1256–1272.
245. Zrehen A, Huttner D. and Meller A, ACS Nano, 2019, 13, 14388–14398. [PubMed: 31756076]
246. Soni GV, Singer A, Yu Z, Sun Y, McNally B. and Meller A, Rev. Sci. Instrum, 2010, 81, 014301. [PubMed: 20113116]
247. Liu S, Wall TA, Ozcelik D, Parks JW, Hawkins AR and Schmidt H, Chem. Commun, 2015, 51, 2084–2087.
248. Assad ON, Di Fiori N, Squires AH and Meller A, Nano Lett, 2015, 15, 745–752. [PubMed: 25522780]
249. Ashkin A, Phys. Rev. Lett, 1970, 24, 156–159.
250. Neuman KC and Block SM, Rev. Sci. Instrum, 2004, 75, 2787–2809. [PubMed: 16878180]
251. Sischka A, Kleimann C, Hachmann W, Schäfer MM, Seuffert I, Tönsing K. and Anselmetti D, Rev. Sci. Instrum, 2008, 79, 063702. [PubMed: 18601408]
252. Nelson EM, Kurz V, Shim J, Timp W. and Timp G, Analyst, 2012, 137, 3020–3027. [PubMed: 22645737]
253. Nimesh S, Halappanavar S, Kaushik NK and Kumar P, Biomed Res. Int, 2015, 2015, 293–306.
254. Kennedy E, Hokmabadi M, Dong Z, McKelvey K, Nelson EM and Timp G, Nano Lett, 2018, 18, 4263–4272. [PubMed: 29870666]
255. Stewart MP, Sharei A, Ding X, Sahay G, Langer R. and Jensen KF, Nature, 2016, 538, 183–192. [PubMed: 27734871]
256. Mejía-Salazar JR and Oliveira ON, Chem. Rev, 2018, 118, 10617–10625. [PubMed: 30247025]
257. Stewart ME, Anderton CR, Thompson LB, Maria J, Gray SK, Rogers JA and Nuzzo RG, Chem. Rev, 2008, 108, 494–521. [PubMed: 18229956]
258. Spitzberg JD, Zrehen A, van Kooten XF and Meller A, Adv. Mater, 2019, 31, 1900422.
259. Amendola V, Pilot R, Frasconi M, Maragò OM and Iatì MA, J. Phys. Condens. Matter, 2017, 29, 203002. [PubMed: 28426435]
260. Homola J, Anal. Bioanal. Chem, 2003, 377, 528–539. [PubMed: 12879189]
261. Ross BM and Lee LP, Nanotechnology, DOI:10.1088/0957-4484/19/27/275201.
262. Jonsson MP and Dekker C, Nano Lett, 2013, 13, 1029–1033. [PubMed: 23402575]
263. Crick CR, Albella P, Ng B, Ivanov AP, Roschuk T, Cecchini MP, Bresme F, Maier SA and Edel JB, Nano Lett, 2015, 15, 553–559. [PubMed: 25467211]

264. Schmidt H. and Hawkins AR, Microfluid. Nanofluidics, 2008, 4, 3–16. [PubMed: 21442048]
265. Yin D, Schmidt H, Barber JP and Hawkins AR, Opt. Express, 2004, 12, 2710. [PubMed: 19475112]
266. Ozcelik D, Parks JW, Wall TA, Stott MA, Cai H, Parks JW, Hawkins AR and Schmidt H, Proc. Natl. Acad. Sci. U. S. A, 2015, 112, 12933–12937. [PubMed: 26438840]
267. Rahman M, Stott MA, Li Y, Hawkins AR and Schmidt H, Optica, 2018, 5, 1311.
268. Kühn S, Phillips BS, Lunt EJ, Hawkins AR and Schmidt H, Lab Chip, 2010, 10, 189–194. [PubMed: 20066246]
269. Kühn S, Measor P, Lunt EJ, Phillips BS, Deamer DW, Hawkins AR and Schmidt H, Lab Chip, 2009, 9, 2212. [PubMed: 19606298]
270. Leake KD, Phillips BS, Yuzvinsky TD, Hawkins AR and Schmidt H, Opt. Express, 2013, 21, 32605. [PubMed: 24514854]
271. Meena GG, Wall TA, Stott MA, Brown O, Robison R, Hawkins AR and Schmidt H, Opt. Express, 2020, 28, 33019. [PubMed: 33114971]
272. Meena GG, Hanson RL, Wood RL, Brown OT, Stott MA, Robison RA, Pitt WG, Woolley AT, Hawkins AR and Schmidt H, Lab Chip, 2020, 20, 3763–3771. [PubMed: 33048071]
273. Stambaugh AM, Stott MA, Meena GG, Tamhankar M, Carrion R, Patterson JL, Hawkins AR and Schmidt H, IEEE J. Sel. Top. Quantum Electron, 2020, 27, 1–6.
274. Liu Q, Wu H, Wu L, Xie X, Kong J, Ye X. and Liu L, PLoS One, 2012, 7, e46014. [PubMed: 23029365]
275. Chen P, Gu J, Brandin E, Kim Y-R, Qiao Wang A. and Branton Daniel, Nano Lett, 2004, 4, 2293–2298. [PubMed: 25221441]
276. Maglia G, Restrepo MR, Mikhailova E. and Bayley H, Proc. Natl. Acad. Sci, 2008, 105, 19720–19725. [PubMed: 19060213]
277. Wanunu M, Morrison W, Rabin Y, Grosberg AY and Meller A, Nat. Nanotechnol, 2010, 5, 160–165. [PubMed: 20023645]
278. Muthukumar M, J. Chem. Phys, DOI:10.1063/1.3429882.
279. Kühn S, Lunt EJ, Phillips BS, Hawkins AR and Schmidt H, Opt. Lett, 2009, 34, 2306. [PubMed: 19649079]
280. Freedman KJ, Otto LM, Ivanov AP, Barik A, Oh S-H and Edel JB, Nat. Commun, 2016, 7, 10217. [PubMed: 26732171]
281. Chuah K, Wu Y, Vivekchand SRC, Gaus K, Reece PJ, Micolich AP and Gooding JJ, Nat. Commun, 2019, 10, 1–9. [PubMed: 30602773]
282. Lu H, Giordano F. and Ning Z, Genomics, Proteomics Bioinforma., 2016, 14, 265–279.
283. Yang AHJ, Moore SD, Schmidt BS, Klug M, Lipson M. and Erickson D, Nature, 2009, 457, 71–75. [PubMed: 19122638]
284. Cohen AE and Moerner WE, Proc. Natl. Acad. Sci. U. S. A, 2006, 103, 4362–4365. [PubMed: 16537418]
285. Roxworthy BJ, Ko KD, Kumar A, Fung KH, Chow EKC, Liu GL, Fang NX and Toussaint KC, Nano Lett, 2012, 12, 796–801. [PubMed: 22208881]
286. Park SE, Georgescu A. and Huh D, Science (80-.)., 2019, 364, 960–965.

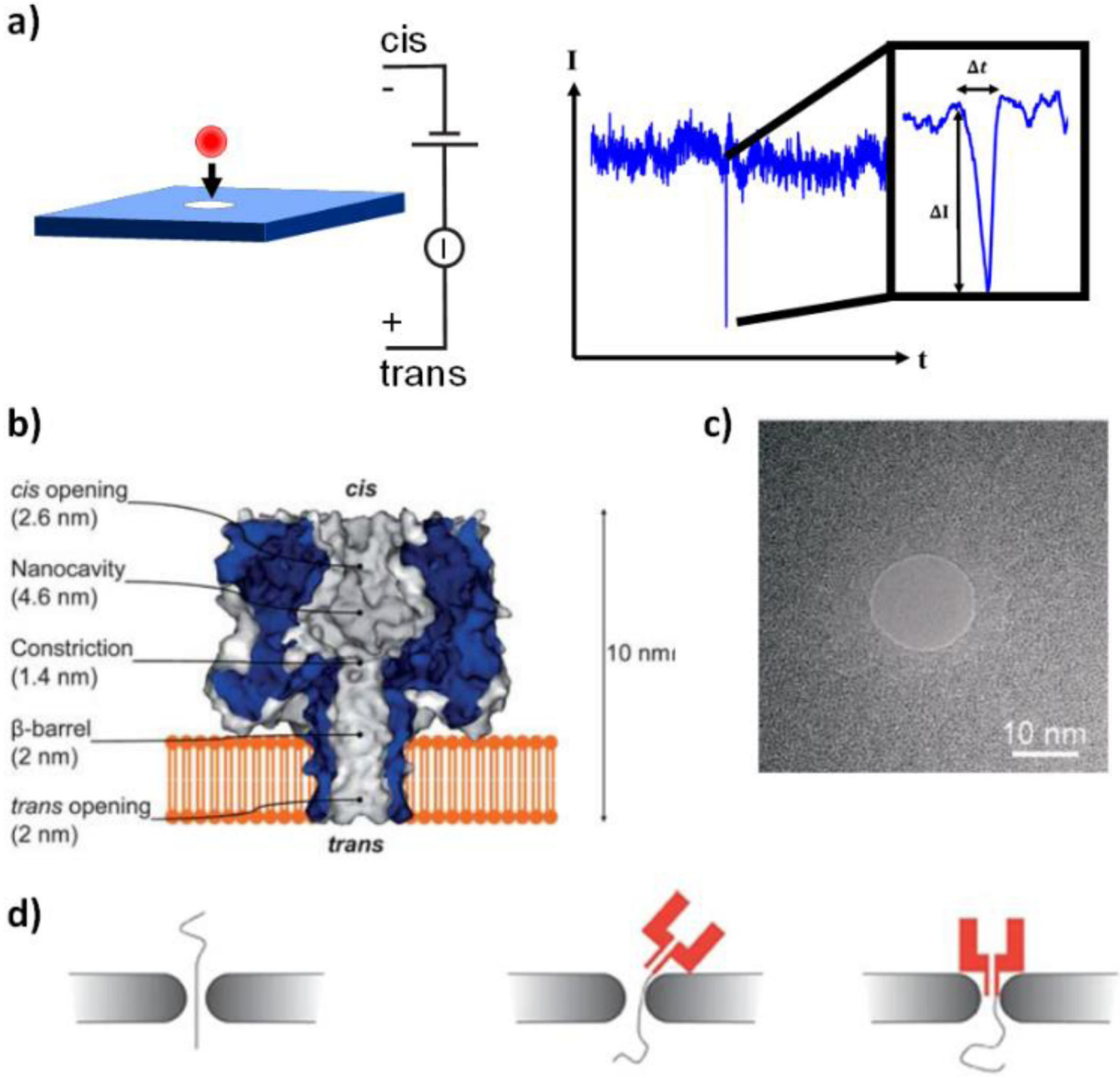

Fig 1.

The working principle and types of nanopore. a) Schematic illustration of nanopore working principle and detection signal. b) Typical cross section of an α-hemolysin pore. Reproduced with permission from ref. 15. c) SEM image of a typical solid-state nanopore. Reproduced with permission from ref. 119. d) Schematic of a hybrid nanopore combining a biological and ss nanopore. Reproduced with permission from ref. 152.

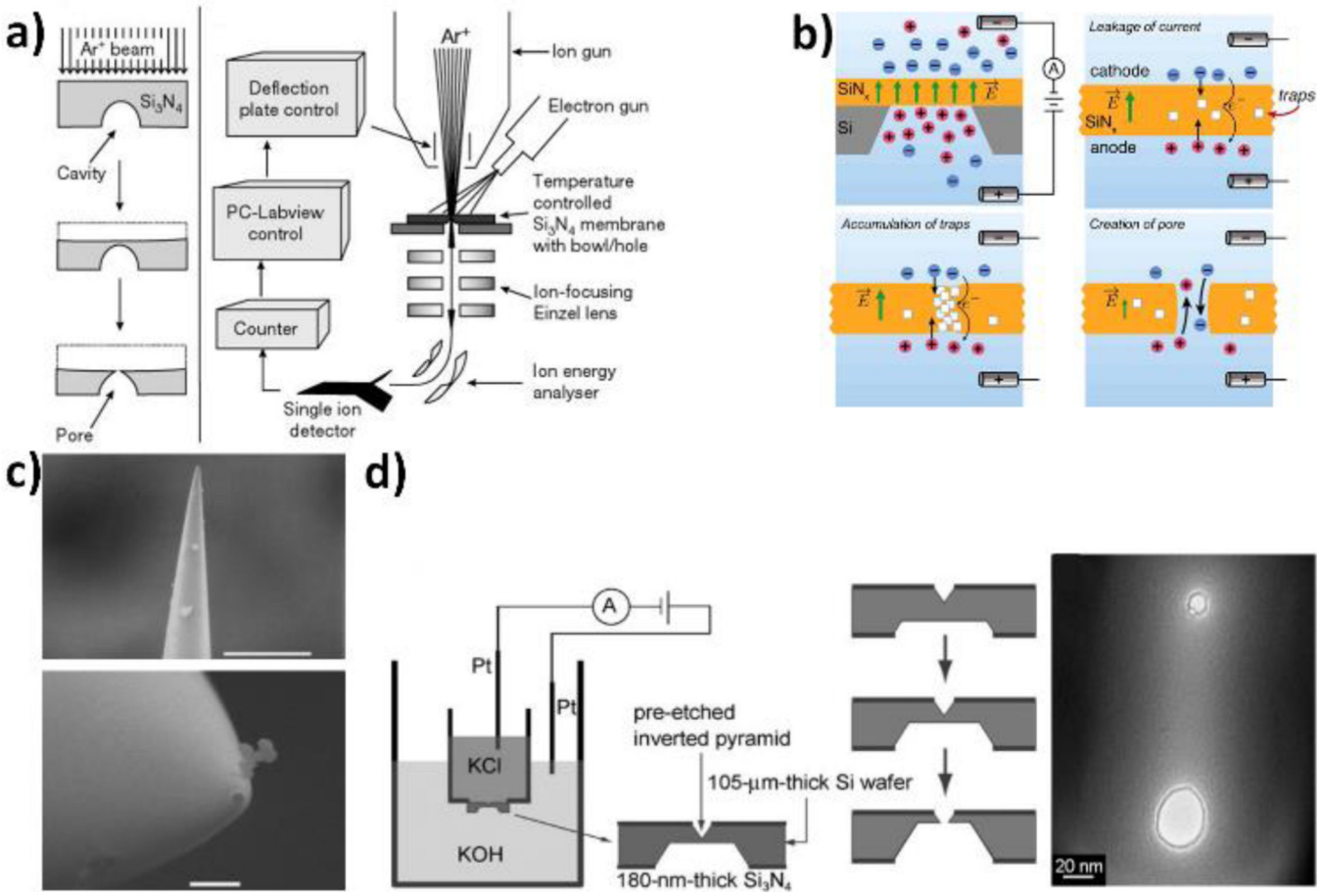

Fig 2.

Different nanopore fabrication techniques. a) Nanopore milling method using feedback-controlled Ion beam sculping. Reproduced with permission from ref. 146. b) Step by step illustration of dielectric breakdown method for nanopore fabrication. Reproduced with permission from ref. 172. c) SEM images of a typical nanopipette (top) scale bar 2 μm and (bottom) 200nm. Reproduced with permission from ref. 181. d) Schematic representation of experimental setup for nanopore fabrication using feedback controlled chemical etching. Reproduced with permission from ref. 187.

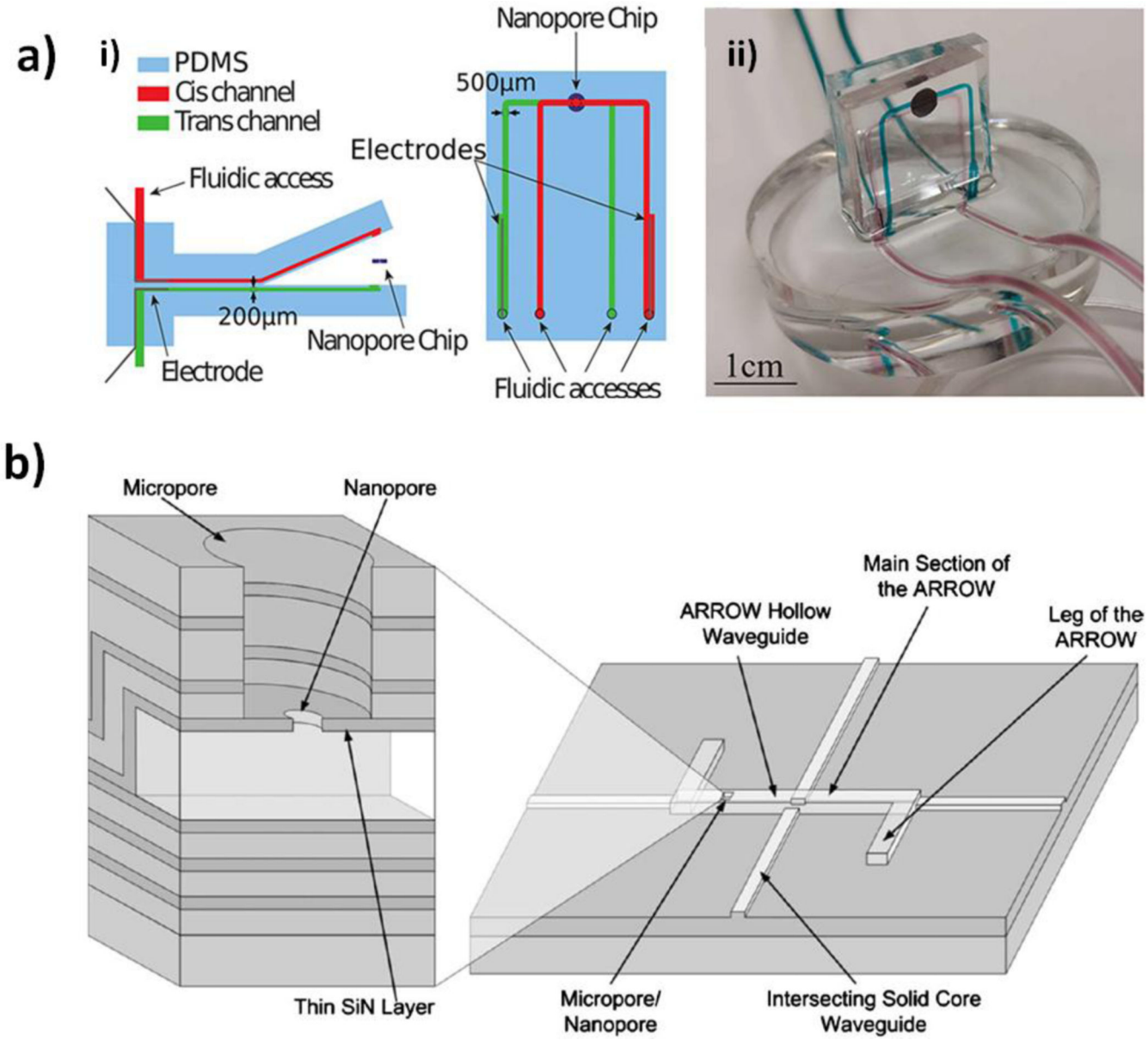

Fig. 3:

Microfluidic integrated nanopore for electrical detection of target particles. a) Reusable nanopore device with microfluidic channels on PDMS. i) Schematic of cross sectional and top view of the device. ii) Photograph of a complete nanopore device with a nanopore chip clamped inside PDMS layers. Reproduced with permission from ref. 93. b) Schematic presentation of a typical ARROW optofluidic device with liquid channel and optical waveguides. Zoomed in image shows cross section view of the micropore and nanopore drilled on the liquid channel. Reproduced with permission from ref. 215.

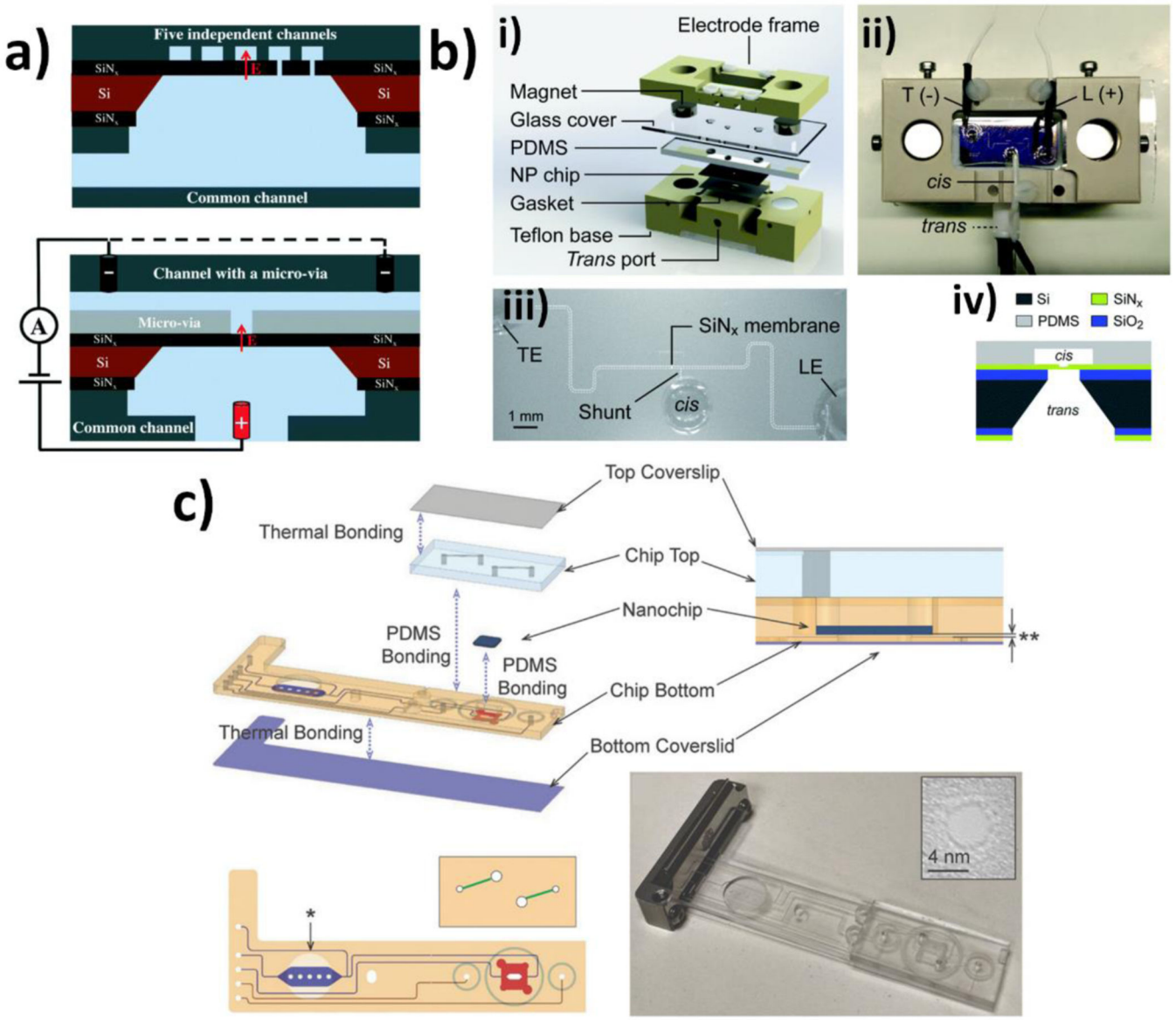

Fig 4.

Microfluidic integrated nanopore with different functionality. a) Multichannel nanopore device with individual channel controllability. Schematic cross-sectional view illustrates the nanopore fabrication process with controlled dielectric breakdown method. An extra electrode as well as micro via can help the fabrication process by providing symmetric electric field. Reproduced with permission from ref. 97. b) Electrokinetic fluidic control on an integrated nanopore device. i) schematic of individual parts of the device. ii) Top view of the complete setup. iii) top view of the nanopore integrated ITP focusing channel. iv) cross sectional schematic of the microfluidic channel and nanopore. Reproduced with permission from ref. 92. c) Schematic of the nanopore integrated microfluidic chip. Top left image shows expanded view of the device components. Top right image shows the cross-sectional view of the nanopore chip with PDMS and zeonex plastic layers. Bottom left image shows top view of the microfluidic device. Bottom right image shows the photograph

of the complete microfluidic device. (Inset) TEM image of the 5nm diameter solid state nanopore. Reproduced with permission from ref. 91.

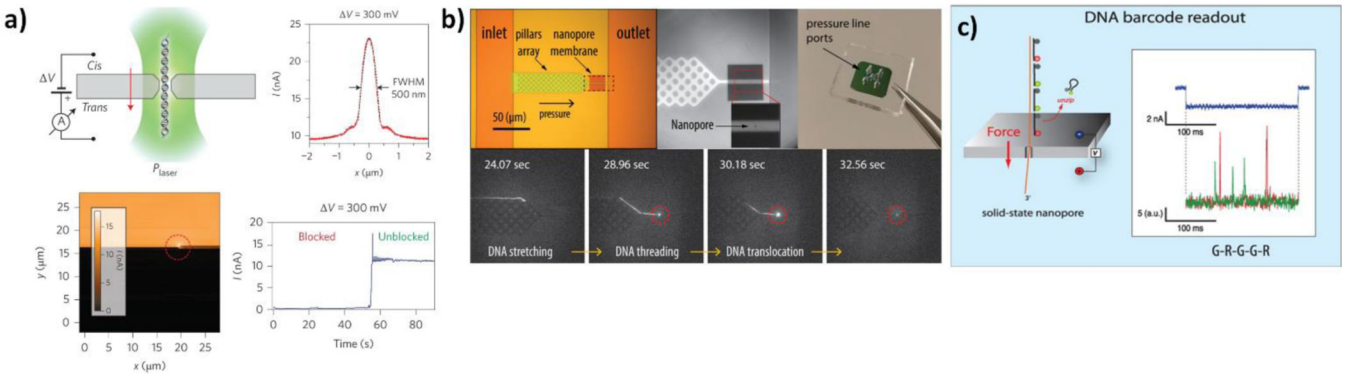

Fig. 5.

Optical integration with nanopore. a) Optoelectronic control of nanopore surface charge. Top left: Schematic view of the optical integration with nanopore where a 532nm wavelength laser beam is focused at the nanopore. This integration influences the translocation characteristics of a target particle. Top right: The ionic current profile with the position of the laser scan in x-axis. Bottom left: The two-dimensional ionic current profile of a clogged nanopore. Right after the laser scan passes the nanopore, it unclogs the nanopore and the nanopore current increases. Bottom right: The nanopore current change with time. The current jumps and stabilizes when the laser beam unclog the pore. Reproduced with permission from ref. 244. b) (Top figures) Bright field image of the device for on chip stretching, sorting and electro-optical detection of ultralong nucleic acid. (Bottom images) Time series photographs of stretching and translocation of optically tagged DNA molecule. Reproduced with permission from ref. 247. c) schematic view of a two-colors (red and green) single fluorophores DNA barcode translocating through the nanopore. The recorded electrical and fluorescent signals show multimodal detection scheme. Reproduced with permission from ref. 250.

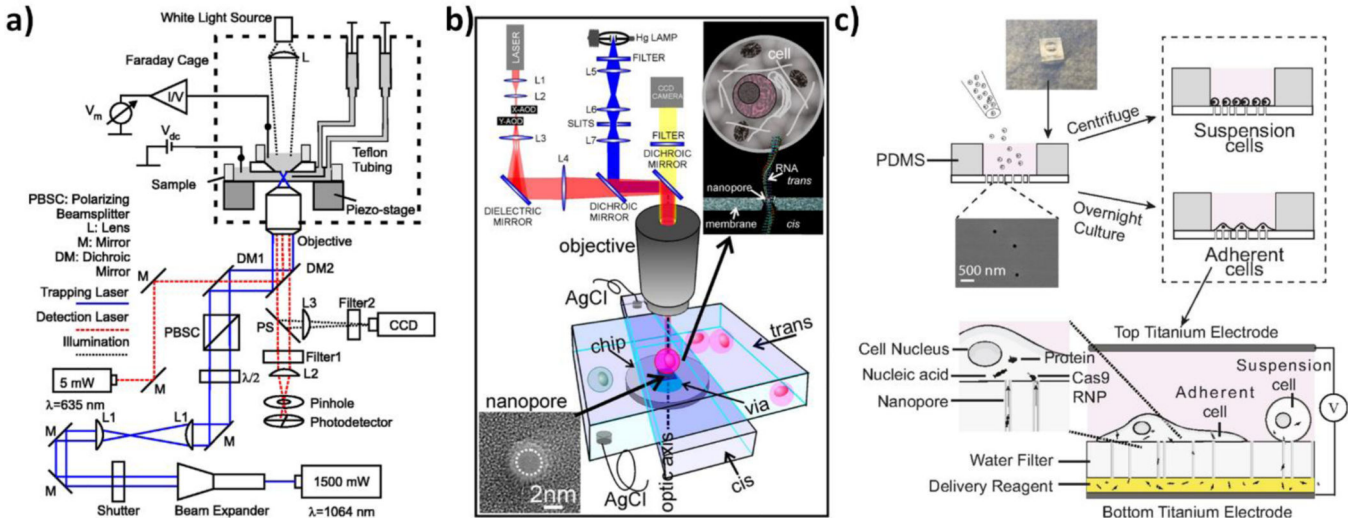

Fig. 6.

Optical tweezer based manipulation on integrated nanopore devices. a) Schematic representation and experimental setup of the experimental setup for nanopore force spectroscopy. Reproduced with permission from ref. 117. b) Schematic of the experimental setup for optical tweezer integrated nanopore based cell transfection device; Zoomed in section shows cross sectional view of the nanopore, on top of which a cell is trapped by optical tweezer and being transfected by RNA molecule. Inset shows a 2.5nm diameter solid state nanopore. Reproduced with permission from ref. 113. c) Top left: Schematic view of nanopore based electroporation device. The SEM image shows ~100nm diameter nanopore distributed in the polycarbonate membrane. This device is applicable for both suspension and adherent cells. Bottom right: The Schematic of Cas-9 RNP and protein delivery process through electroporation method. Reproduced with permission from ref. 114.

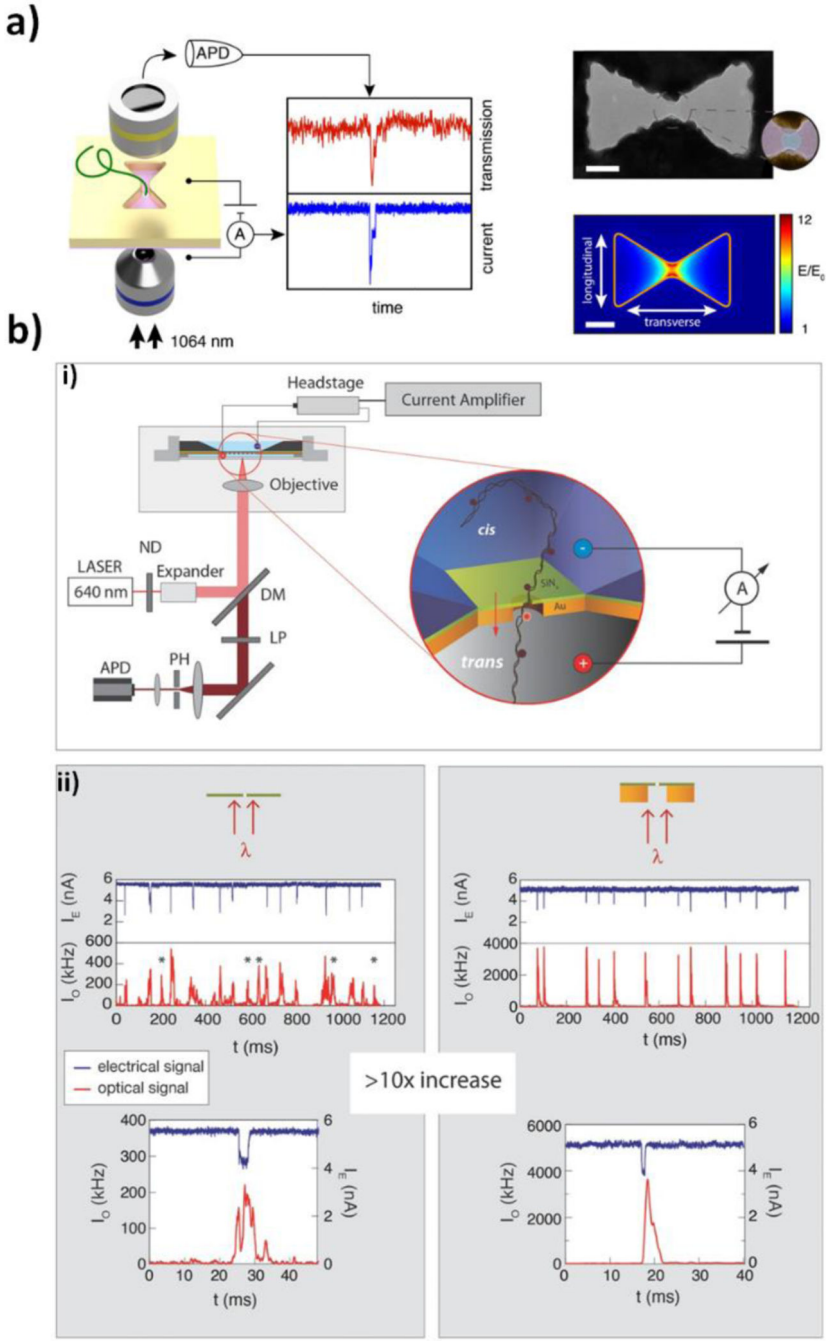

Fig. 7.

Plasmonic nanopores. a) (Left) Schematic of inverted bowtie nanopore for label free particle detection. The optical transmission plot and nanopore current trace confirms simultaneous detection of a target particle. (Top right) TEM photograph of the inverted bow structure with a nanopore at the center. (Bottom right) Normalized electric field plot, simulated for the structure shown in the top right plot. Reproduced with permission from ref. 110. b) Simultaneous electro optical detection of labeled particle in a nanopore integrated plasmonic nano well (NP-PNW). i) Schematic of the experimental setup. ii) Comparison between

electrical and optical signals obtained from standard nanopore device and NP-PNW device. Reproduced with permission from ref. 111.

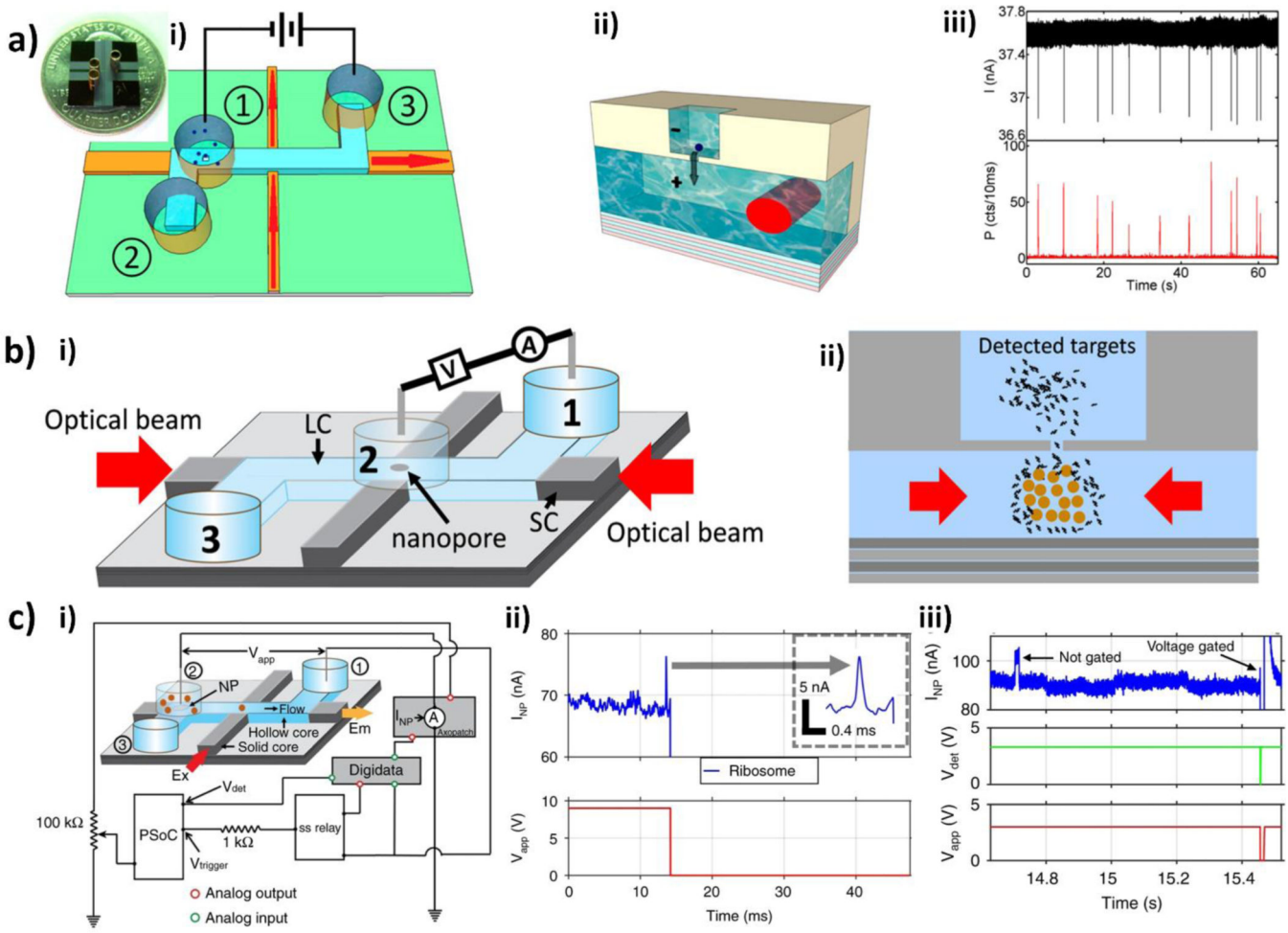

Fig. 8.

Optofluidic integration with nanopore. a) Simultaneous electro-optical detection of single molecules in an optofluidic device. i) Schematic representation of the setup on an ARROW optofluidic device. ii) Cross-section of the nanopore and LC channel for visualization of the electro-optical detection methodology. iii) Actual electrical (black) and optical (red) trace of single H1N1 influenza virus detection. Reproduced with permission from ref. 52. b) Trap assisted capture rate enhancement of a nanopore. i) Schematic illustration of the experimental setup. ii) A cartoon depicting the conceptual visualization of TACRE. Reproduced with permission from ref. 95. c) On demand target delivery on a programmable ARROW optofluidic device. i) Schematic illustration with feedback control mechanism. ii) Current (top) and voltage (bottom) trace of a voltage gated single ribosome delivery. iii) Current (top), identification signal (middle) and voltage (bottom) trace of identification and voltage gating of only λ-DNAs from a mixture of λ-DNA and ribosome. Reproduced with permission from ref. 45.